Analyzing and Classifying Neural Dynamics from Intracranial Electroencephalography Signals in Brain-Computer Interface Applications

Naresh Nagabushan

Thesis submitted to the Faculty of the

Virginia Polytechnic Institute and State University

in partial fulfillment of the requirements for the degree of

Master of Science

in

Computer Engineering

Pratap Tokekar, Chair

Sujith Vijayan, Co-chair

Amos L. Abbott

May 8, 2019

Blacksburg, Virginia

Keywords: Brain Computer Interfaces, Signal Processing, Electroencephalography, Machine Learning.

Analyzing and Classifying Neural Dynamics from Intracranial Electroencephalography Signals in Brain-Computer Interface Applications

Naresh Nagabushan

(ABSTRACT)

Brain-Computer Interfaces (BCIs) that rely on motor imagery currently allow subjects to control quad-copters, robotic arms, and computer cursors. Recent advancements have been made possible because of breakthroughs in fields such as electrical engineering, computer science, and neuroscience. Currently, most real-time BCIs use hand-crafted feature extractors, feature selectors, and classification algorithms. In this work, we explore the different classification algorithms currently used in electroencephalographic (EEG) signal classification and assess their performance on intracranial EEG (iEEG) data. We first discuss the motor imagery task employed using iEEG signals and find features that clearly distinguish between different classes. Second, we compare the different state-of-the-art classifiers used in EEG BCIs in terms of their error rate, computational requirements, and feature interpret-ability. Next, we show the effectiveness of these classifiers in iEEG BCIs and last, show that our new classification algorithm that is designed to use spatial, spectral, and temporal information reaches performance comparable to other state-of-the-art classifiers while also allowing increased feature interpret-ability.

Analyzing and Classifying Neural Dynamics from Intracranial Electroencephalography Signals in Brain-Computer Interface Applications

Naresh Nagabushan

(GENERAL AUDIENCE ABSTRACT)

Brain-Computer Interfaces (BCIs) as the name suggests allows individuals to interact with computers using electrical activity captured from different regions of the brain. These devices have been shown to allows subjects to control a number of devices such as quad-copters, robotic arms, and computer cursors. Applications such as these obtain electrical signals from the brain using electrodes either placed non-invasively on the scalp (also known as an electroencephalographic signal, EEG) or invasively on the surface of the brain (Electrocorticographic signal, ECoG). Before a participant can effectively communicate with the computer, the computer is calibrated to recognize different signals by collecting data from the subject and learning to distinguish them using a classification algorithm. In this work, we were interested in analyzing the effectiveness of using signals obtained from deep brain structures by using electrodes place invasively (also known as intracranial EEG, iEEG). We collected iEEG data during a two hand movement task and manually analyzed the data to find regions of the brain that are most effective in allowing us to distinguish signals during movements. We later showed that this task could be automated by using classification algorithms that are borrowed from electroencephalographic (EEG) signal experiments.

Dedication

This work is dedicated to the open source community.

Acknowledgments

Research isn't easy, there are a lot of lows and very little highs. But, the lows are what makes the highs worth doing it all over again. I would like to thank my advisor Dr. Sujith Vijayan for instilling this thought right from the very beginning and encouraging me during this entire process. I am also very grateful to my committee members Dr. Pratap Tokekar and Dr. Lynn Abbott for taking the time to sit down and brainstorm my ideas.

Contents

List of Figures viii

List of Tables xi

1 Introduction 1

2 Previous Work 7

3 iEEG Motor Imagery Task: Implementation Details 9

3.1 BCI Experiment Overview 9

3.2 Stage 1: Calibration Stage 12

3.3 Stage 2: Training Stage 13

3.4 Stage 3: Online Stage 14

4 iEEG Motor Imagery Task: Relevant Feature Estimation 16

4.1 Subject description 16

4.2 Feature Estimation 18

4.2.1 Spatial and Spectral Features 19

4.2.2 Temporal Features 23

5 EEG Signal Classifiers 27

5.1 Previous methods 28
5.1.1 Common Spatial Pattern 28
5.1.2 Filter Bank Common Spatial pattern 29
5.1.3 Deep4Net 29
5.1.4 EEGNet 30
5.2 EphysNet 30
5.3 EEG dataset description and experimental setup 33
5.4 EEG Motor Imagery Classification Results 33
5.5 Feature Visualization 34

6 iEEG Signal Classifiers **40**
6.1 Experimental Setup 40
6.2 iEEG Motor Imagery Classification Results 42
6.3 Feature Visualization 44

7 Conclusions and Future Work **48**

Bibliography **50**

Appendix A **56**

List of Figures

1.1 Stage 1 and Stage 3 BCI block diagrams 2

3.1 The acquisition machine (Pegasus Machine) connects to the Neuralynx amplifier and streams data over the local network. The presentation machine reads data from the iEEG stream, classifies the signals, and presents the control signal, which also provides feedback for the BCI application. 10

3.2 Visual cues as seen by the subject during the calibration stage 12

3.3 Visual Cues as seen by each subject during the online stage 14

4.1 Electrode map of subject CAR 10. The colored dots indicate the location of the electrode contacts with the same color assigned to electrode contacts in the same depth electrode. 17

4.2 CAR 04 power and power significance plots 20

4.3 Power spectrum during left- and right-hand movements in both hemispheres for subjects CAR04 and CAR10 21

4.4 Spectrogram at one of the hippocampal electrodes in CAR04 showing the difference at both low and high frequencies between imagination of left- and right-hand movements. 24

4.5 The average cross correlation between low and high frequency components during both left and right movements 26

5.1 EphysNet Block Diagram used in EEG signal classification. Boxes in orange indicate the kernels applied at each stage. 31

5.2 Visualizing Bandpass Convolutional Kernels: Top row represents the bandpass kernels learnt by EphyNet and the bottom row represents the power spectral density of the kernel above it for subject 3 during 2 hand motor imagery 35

5.3 Visualizing Spectral Filters: Top row shows the first 4 bandpass kernels learnt by EphysNet o subject 3. The second row shows the power spectral density of the kernels above it. The last four rows show the spatial filters learnt using each of the bandpass filters above it. 37

5.4 SHAP based feature visualization: Top row shows the raw signals at all channels for subject 3 during left hand movement along with its importance values towards its right. The topoplot consists of the average of importance values assigned during the left hand movement time samples. Bottom row indicates the same thing but for the right trials. Both the left and right trials are 1s segments from [-0.5, 0.5]s 38

5.5 SHAP based feature visualization to track features: Left Column shows the raw eeg traces along a continuous set of data 1s long data chunks. The right column shows the SHAP values of the chunks towards their left.The signal moves forward in time as we proceed from the top to the bottom row. 39

6.1 EphysNet when applied to iEEG data. The sizes of feature map after each layer is indicatd along with the kernel shapes used in each layer with orange boxes. 41

6.2 Visualizing Bandpass Convolutional Kernels: The top row shows the raw bandpass kernel values learnt by EPhysNet along with its power spectral density in the bottom row. 45

6.3 SHAP based feature visualization: Top row shows the raw iEEG data along all the 64 channels from [-0.1, 0.9]s during the left trial as an image along with its corresponding SHAP values towards its right. The Average SHAP values in movement window in shown towards the extreme right. Bottom row depicts a similar observatino during the right trial. The iEEG channels are visible when zooming in on the digital version. 46

6.4 SHAP based feature visualization: Left column shows 10 consecutive (top to bottom) raw iEEG traces as image and the right column shows its corresponding SHAP values. All chunks were obtained during right hand movement from subject CAR08. 47

A.1 CAR 10 Hilbert power and Hilbert Power Significance plots 56

A.2 CAR 08 Hilbert power and Hilbert Power Significance plots 57

List of Tables

4.1 Information regarding each of the 7 subjects involved in the intracranial EEG study 18

5.1 EphysNet Model Architecture. BS is the batch size 32

5.2 Number of model parameters when using Deep4Net, EEGNet and EphysNet on EEG motor imagery data 32

5.3 Test Accuracy along with the standard deviation after training CSP, FBCSP, Deep4Net, EEGNet and EphysNet on all the 9 EEG subjects. The values highlighted indicates a significantly higher ($p<0.05$) test accuracy when compared to the other classifiers 34

6.1 Number of model parameters when using Deep4Net, EEGNet and EphysNet on iEEG motor imagery data 40

6.2 EphysNet Model Architecture. BS is the batch size 41

6.3 Test Accuracies after 10 repeats on four classifiers when applied to iEEG Motor Imagery Task. FBCSP is excluded from analysis as it was not possible to increase its classification accuracy beyond chance on any of the subjects. Bold values indicates stastically significant results ($p<0.05$) 42

List of Abbreviations

BCI Brain Computer Interface

ECoG Electrocorticography

EEG Electroencephalography

ERD Event Related Desynchronization

ERS Event Related Synchronization

iEEG Intracranial Electroencephalography

Chapter 1

Introduction

Brain-Computer Interfaces (BCIs) allow individuals to control external devices such as robotic arms ([45], [13]), electric wheelchairs ([42], [35]), and even quad-copters ([18]) by modulating their neural activity. They work by collecting neurophysiological signals directly from the brain and mapping these signals to the user's intents. Recently, BCIs have seen increasing applications such as enabling disabled individuals to control motor prosthetics ([42]), allowing users to control input in the gaming industry ([23]), and enabling individuals to control applications in a variety of other contexts ([6], [29], [1], [15], [24]).

BCI systems are typically divided into three stages. Stage 1, also known as the offline signal acquisition stage (see Fig. 1.1a), collects calibration data to train a classification algorithm that can learn a mapping between brain signals and classes (i.e., the desired set of actions). Based on the types of electrodes used during this stage, BCIs can broadly be divided into invasive and non-invasive methods. Invasive methods use electrodes that are either placed on the surface of the cortex (Electrocorticography, ECoG) or penetrate the cortex; the latter are either depth electrodes, hybrid depth electrodes, or microelectrodes that can record from an individual neuron or small group of neurons (Local Field Potentials, LFPs). Noninvasive techniques, on the other hand, use electrodes placed on the scalp (Electroencephalography, EEG). The classes, depending on the BCI application, can be different imagined movements ([22]) such as left hand, right hand, both feet, or both hands. The signals associated with the imagined movements could be, among other things, Event-Related Potentials (ERPs,

(a) Stage 1: Offline signal acquisition stage.

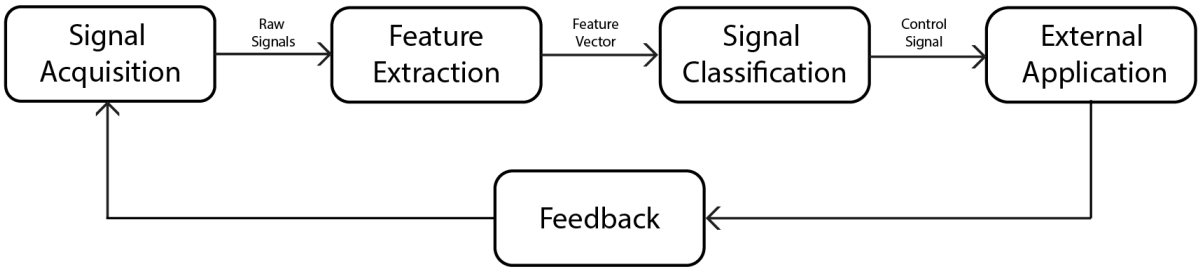

(b) Stage 3: Online stage indicating the different stages along with the output from each stage.

Figure 1.1: Stage 1 and Stage 3 BCI block diagrams

[33]) or Event Related Negativity (ERNs, [28]). The user is usually shown different visual stimuli and data from all the electrodes along with the stimulus is recorded onto an external device as shown in Fig. 1.1a.

Stage 2, also known as the training stage, uses the calibration data collected in Stage 1 in order to find relevant feature vectors that discriminate data between different classes. The features extracted here are usually in the form of a vector of numbers when using a classifier or some other signal characteristic (known as the feature vector) and have a lower dimensionality when compared to raw signals. Reducing the dimensionality of features allows us to use a lower number of training samples to train the classifier. This is especially useful in BCIs as acquiring a large number of training examples from an individual is time-consuming. These lower dimensional feature vectors are then used to train classification algorithms that maps feature vectors onto different classes.

The online stage, Stage 3 (see Fig. 1.1b), allows the user to control an external application by modulating their neural activity. This stage generally has 5 blocks. The first block, known as signal acquisition, as the name suggests acquires neural signals from the user. The second block, known as the feature extraction block, preprocesses the signals from the previous block and uses the feature extractors from Stage 2 to obtain the relevant features from the data. Features extracted in this block are then used in block 3 (the classification block), which maps the feature vectors to one of the possible classes. An external application uses the control signals (classification outputs) to perform an action such as control an arm or a computer cursor. Since BCIs typically have two control mechanisms, the user and the feature extractor/classifier, after the control signals are sent to the external application, the user can change the way neural signals are modulated by employing feedback (e.g., the direction a cursor is moving across a screen) in order to perform better.

As an example, consider 2D motor imagery-based BCIs using EEG signals to move a cursor

left, right, up, or down. Stage 1 acquires ([36]) EEG signals while the subject imagines, for instance, moving their left arm, right arm, both feet, or both arms. In stage 2, the recorded EEG data is then used to train a feature extractor and classifier that maps the EEG signals of each imagined movement to one of the four classes, for example, imagined left-hand movement to left class, right hand to right class, both feet to down class and both hands to up class. Finally in stage 3, the classification results can then be fed as control signals to an external application to control the 2D movement of a cursor.

Inspired by recent advances, in this work, we have used intracranial electroencephalographic (iEEG) data, collected using depth electrodes, in a two class BCI task using motor imagery. We first performed a thorough data analysis to manually find features that discriminated between the two motor imagery classes after the offline data acquisition stage and later implemented the training stage with the aim of automatically finding good features from raw data. We also compared various state of the art EEG classification algorithms along with our own classifier for iEEG data and also explored the features learned by our classifier.

Non invasive BCIs using EEG have several limitations ([37], [38]) such as:

- low signal amplitude (10-20 μV) when compared with invasive techniques such as ECoG or iEEG (50-100 μV)
- low spatial resolution, a few centimeters in non invasive vs a few millimeters in invasive techniques
- higher vulnerability to Electrooculograph (EOG) and Electromyograph (EMG) artifacts
- lower frequency range (0-40Hz) when compared with invasive techniques that can record frequencies up to several kiloHertz

The advantages of invasive BCIs clearly seem to make them a better alternative to EEGs with respect to signal quality and the information content in the signal ([38], [37]). The only major downside is the risk associated with undergoing surgery in order to implant recording electrodes. This limitation makes BCI applications with invasive methodologies extremely rare in humans and is currently possible only in human subjects who have electrodes implanted for clinical reasons.

A good BCI system needs to automatically find discriminative information in order to distinguish between different classes in a BCI task. Most of the current studies ([38], [20], [21]) that perform BCI tasks using invasive techniques rely on manual data analysis and counterintuitive subject tasks to find clearly discriminative features; these tasks can include things such as saying words or protruding the tongue in order to move a cursor. A number of EEG BCI studies have shown that machine learning models such as CSP [46] and FBCSP [2] along with deep learning based methods such as EEGNet [19] and Deep4Net [39] can automatically find discriminative features for classifying data. Deep learning models extract relevant features by learning directly from raw data (with mean subtraction and bandpassing between 0-40Hz). Deep4Net and EEGNet models have also been designed to learn features with relatively minimal amounts of data and also to use as little computational resources during the online phase as possible when compared with CSP and FBCSP. Inspired by these advances in EEG signal classification, we have applied a number of classical machine learning and deep learning techniques from EEG classification onto iEEG signals and have assessed their performance on our dataset collected using depth electrodes in a binary motor imagery task.

Since deep learning models have been known as black boxes that make it hard for researchers to visualize the features learned, we also aim to provide a detailed feature analysis for all the models used in both the EEG and invasive datasets in this work. In order to get an

estimate of some of the good features that must be learned to classify between left and right hand motor imagery in iEEG data, we perform a thorough data analysis to find the relevant frequency bands, relevant regions (electrodes) and cross co-variance between left and right hand movements that might give good results in BCI experiments.

We have made three main contributions in this work:

1. We have implemented an entire BCI experimental pipeline that allows data to be collected during Stage 1, allows classifiers to be trained using either MATLAB or Python during Stage 2, and also allows the trained classifiers to be used during an online experiment in Stage 3 (Sec. 3).

2. We collected iEEG data from 7 subjects during a two hand motor imagery task and later performed a thorough data analysis in order to determine the most useful spatial, spectral, and temporal features (Sec. 4).

3. Finally, we have implemented a novel classification algorithm that learns to classify iEEG data end-to-end and compared its performance in EEG (Sec. 5) and iEEG data (6) during two hand motor imagery. Features learned by the new classification algorithm have also been discussed in Sec. 5 and Sec. 6.

Chapter 2

Previous Work

In this section, we discuss some of the previous efforts done in classifying electrophysiological data from the brain using automated techniques and also previous work involved in using invasive signal acquisition techniques in order to perform a BCI task.

[20] is one of the earliest efforts in using invasive ECoG data in BCIs. The authors had shown the by using ECoG signals a subject could perform a 1D movement task after only about 3-24 minutes of training. The features used to control the cursor were manually selected for each subject and the tasks performed by each subject were counterintuitive such as saying words and protruding the tongue. The authors in [38], for the first time showed that 2D motor control could be achieved using ECoG data to control a computer cursor, but, features were still selected manually for each individual when preforming counterintutive tasks. In this work, we are interested in determining if automatic feature extraction techniques could be used in intracranial EEG data. Since, intracranial EEG is obtained from electrodes placed within deep brain structures and not the surface of the cortex like in ECoG, the amount of literature available that analyses iEEG is limited. Most of the literature on using intracranial EEG comes from work on detecting of interictal epileptic discharges ([44], [3]). The authors here, used a variety of deep learning algorithms to detect the presence of interictal epileptic discharge, but did not analyze iEEG features during a BCI task. The authors in [45], demonstrated that using signals from a group of neurons allowed them to encode arm movements thereby allowing an individual to control a robotic arm. This study

also uses specific regions of the brain and specific frequency ranges to select desired features and is different from our work which aims to automatically extract features from raw iEEG data.

Because of the limited amount of literature available for invasive BCIs and almost no previous work done in using iEEG for BCIs, we turned to the EEG literature to help find classification algorithms that could help extract features from the raw data. Because of its non invasive nature there has been a lot of research done on using EEG for Brain Computer Interfaces. The authors in [2], showed that using Common Spatial Pattern [46] on a number of different bandpassed input signals and then using a feature selection algorithm to select relevant features could perform well on data used at a BCI competition [43] which had 4 motor imagery classes. The authors in [39], showed that one could use an end-to-end deep learning algorithm that learns directly from raw EEG data to perform motor imagery tasks and reach FBCSP performance. Using a variety of feature visualization techniques, they were also able to visualize the features learned by their classifier. The authors in [19], used a similar technique as in [39], but replaced convolutions layers with depth-wise separable convolutions along with other modifications to implement a classification algorithm that performed well in a variety of BCI task settings such as P300 spellers [12], Error Related Negativity (ERN) [10] and motor imagery. The authors were also able to show the features used during each paradigm using a variety of techniques. Inspired by these papers, here we implemented a classification algorithm that classifies iEEG data during motor imagery tasks and have also applied a number of feature visualization techniques to find the features used during classification. We have also manually analyzed the iEEG data in order to determine the most important features that helps discriminate between classes and verified if our classification algorithm was able to automatically learn them.

Chapter 3

iEEG Motor Imagery Task: Implementation Details

In this section, we describe the experimental setup we used to collect iEEG data during the different stages of our motor imagery task. We start with an overview of the BCI experiment along with a brief description of the experimental hardware setup and later give a detailed description of each stage used in the experiment.

3.1 BCI Experiment Overview

An online BCI experiment mainly consists of three stages. In the calibration stage (Stage 1), the subjects are shown markers on the screen and asked to imagine a specific movement based on the instructions shown. The training stage (Stage 2) uses data collected in Stage 1 to find features in the iEEG data that clearly distinguish between motor imagery tasks (left and right hand movement in our case). This is done either manually by looking at an r^2 feature plot (r^2 vs frequency vs channel) or automatically by using a classifier that learns a spatial filter and classifier weights. Finally, the online stage (Stage 3) allows the user to control a BCI feedback application (computer cursor in our case) by modulating their neural activity by imagining motor movements. Stage 3 uses the trained classifier from stage 2 to distinguish between different motor imagery categories by classifying the associated neural

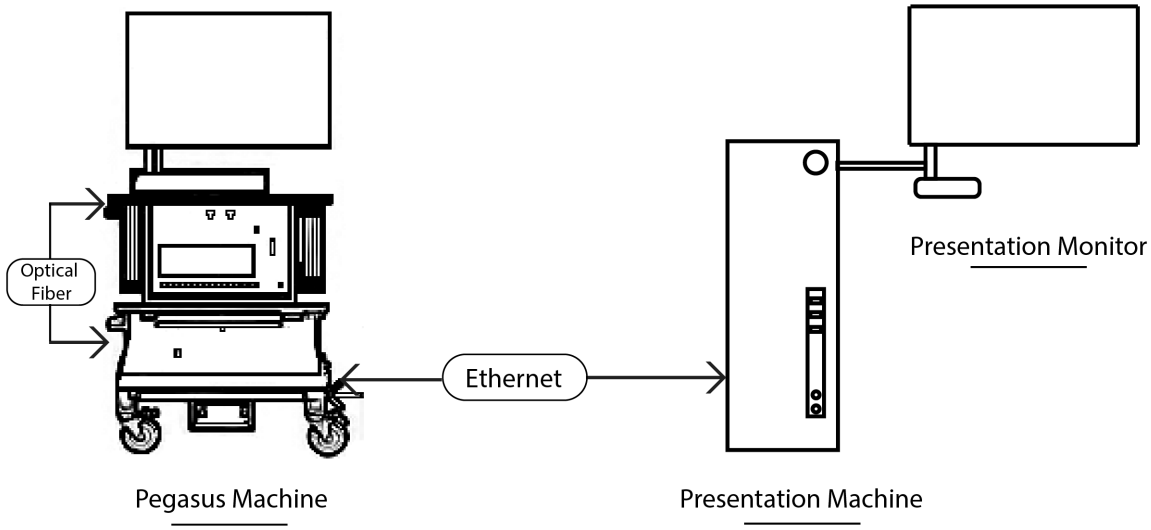

Figure 3.1: The acquisition machine (Pegasus Machine) connects to the Neuralynx amplifier and streams data over the local network. The presentation machine reads data from the iEEG stream, classifies the signals, and presents the control signal, which also provides feedback for the BCI application.

signals in real time to generate control signals and then passes the control signals onto the feedback application.

In order to ensure reliable data collection and training mechanisms, we conducted the experiment using two different PCs, each having a specific role (see Fig. 3.1). The first one of these machines, called the Pegasus Machine, is responsible for collecting data from the amplifier and streaming this data over a local LAN network. The other PC, known as the Presentation Machine, is responsible for collecting the iEEG data streams from each of the channels, training a classifier using this collected data, and presenting feedback during stage 3 (i.e., moving the cursor on the screen to the left or right).

We used the Digital Lynx 16SX amplifier from Neuralynx and connected it to the Pegasus Machine using an optical fiber cable and used an ethernet cable to connect the Pegasus Machine to the Presentation Machine. The Pegasus Machine uses the Pegasus Acquisition Software from Neuralynx to communicate with the amplifier and to stream data from it. Using the Pegasus Acquisition Software, we created a local data stream on the Pegasus Machine and used the ethernet cable to stream data to the Presentation Machine. We decided to only use wired connections to ensure that there were no dropped connections during the experiment and to also avoid any unnecessary latencies introduced by a wireless connection. The Presentation machine collected the data streams using FieldTrip [30], which internally uses the MATLAB-Netcom client API provided by Neuralynx.

We ensured that the latency was kept under 30ms during the entire experiment by limiting the number of channel streams to 64 and by downsampling the signals from 32kHz to 2kHz. Data from the Pegasus Machine was sent to the Presentation machine in chunks of 512 timesteps, where each timestep contained data from 64 channels. The TTL pulses that indicated the start of each trial, the point when the motor imagery was performed during each trial, and the end of each trial were sent from the Presentation Machine to the Pegasus

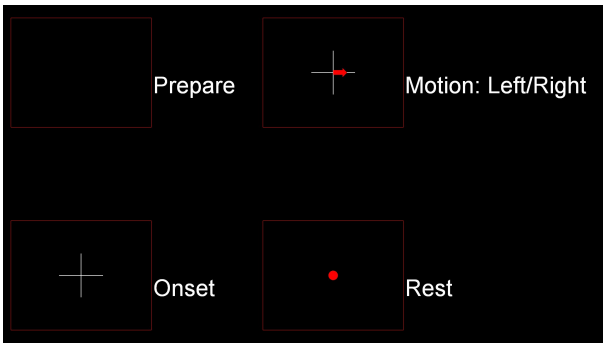

(a) Instructions Screen

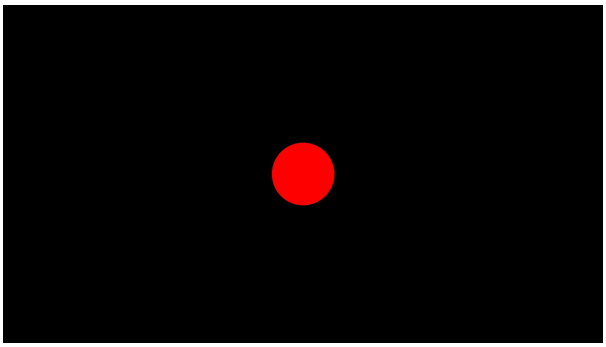

(b) Rest Screen

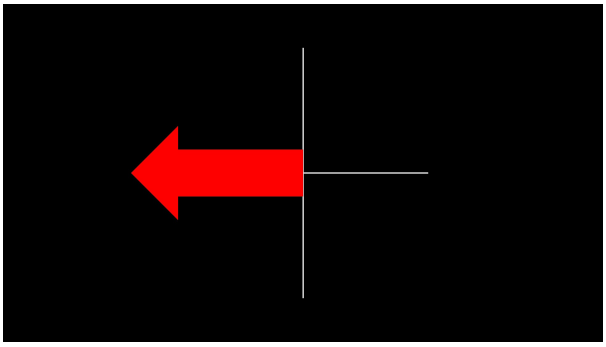

(c) Left Hand Imagery Screen

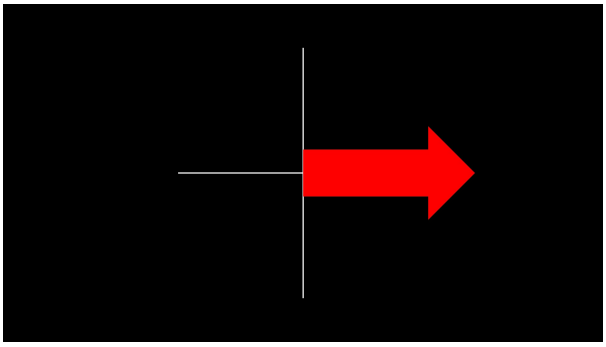

(d) Right Hand Imagery Screen

Figure 3.2: Visual cues as seen by the subject during the calibration stage

Machine using the ethernet cable.

We now give a detailed description of each of the three stages of the iEEG BCI task below.

3.2 Stage 1: Calibration Stage

BCIs need a way to distinguish signals from each imagined motor movement. This is usually done by either manually selecting signal characteristics that show a clear distinction between the motor imagery task and the rest period or by training a classification algorithm that can accurately classify user intents. In order to select appropriate signal characteristics or to train a classification algorithm, we need to collect training data. This is done during the calibration stage.

During this stage, the user is first shown the instructions screen on the Presentation monitor, which is about 80-100 cm away. The instruction screen (Fig. 3.2a) clearly illustrates the motor imagery task to be performed and the visual cue that will indicate the start of each motor imagery trial. The user is shown a red circle to indicate a rest trial (Fig. 3.2b), a red left arrow to indicate they should imagine squeezing their left hand (Fig. 3.2c), and a red right arrow to indicate they should imagine squeezing their right hand (Fig. 3.2d). Each left or right trial lasts for 4s and the rest trial lasts for 2s. The TTL pulses corresponding to each of the trials are transmitted from the Presentation machine to the Pegasus Machine, which stores the TTL pulses along with the raw data from the trial.

3.3 Stage 2: Training Stage

During this stage, the Presentation machine reads the events file along with the neuralynx iEEG data file on the Pegasus Machine. The Presentation Machine uses the events file to appropriately segment each trial. It also preprocesses the iEEG trace by removing line noise using a notch filter at 60Hz and performs common average referencing [25] to eliminate any movement artifacts and increase the signal-to-noise ratio.

Each trial is then chunked into 1s long overlapping segments with an overlap ratio of 96.875%; this gives about 32 samples for every 1s chunk of data (assuming it is padded with zeros). The data from 10% of the trials are converted into testing data and the rest of the trials are used as training and validation. Depending on the classification algorithm used, this data is preprocessed further by band-passing between appropriate frequencies or is directly fed to the classifiers. We discuss this further in Sec. 5. The trained classifier is then saved locally on the Presentation machine to be used in stage 3 (the online stage).

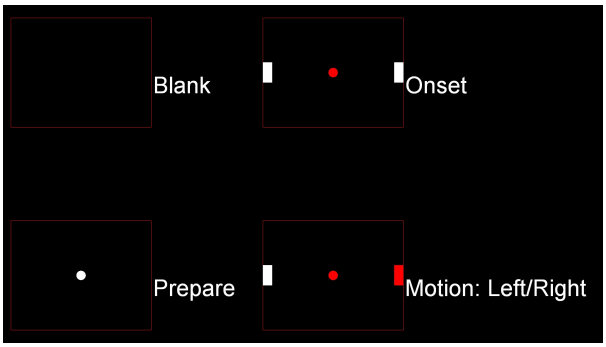

(a) Instructions Screen

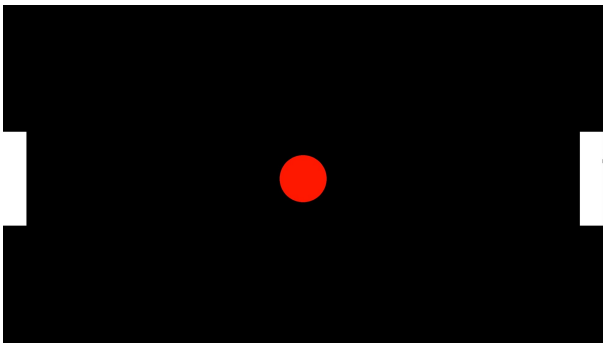

(b) Trial Onset

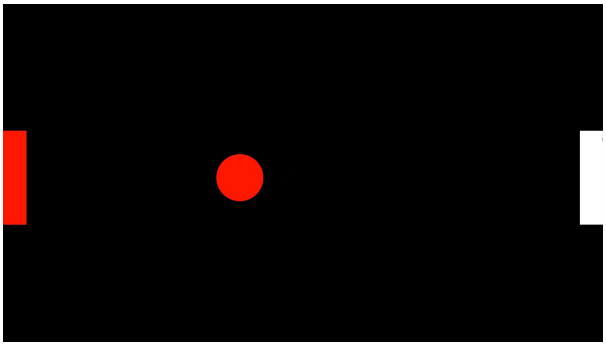

(c) Cursor movement towards the left

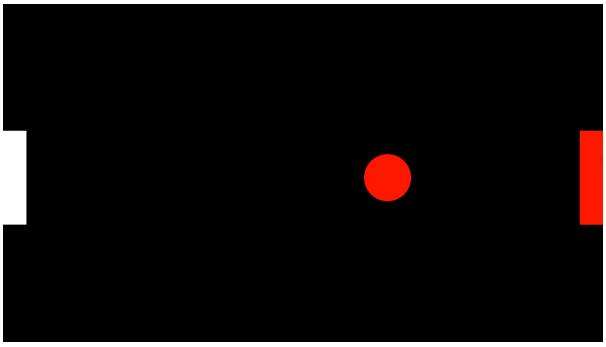

(d) Cursor movement towards the right

Figure 3.3: Visual Cues as seen by each subject during the online stage

3.4 Stage 3: Online Stage

During this stage, the subject gets to control the cursor on-screen to move it to the desired target. Each experiment starts off by first showing an instructions screen. The instructions screen here contains the preparation period display, where the cursor is white and the targets are invisible; this indicates the beginning of a new trial (see Fig. 3.3a). The instructions screen also shows the onset phase display, where both the targets are white (see Fig. 3.3b) and lastly, a right/left target display, wherein the target is highlighted in red (see Fig. 3.3c and Fig. 3.3d). The subject is given a maximum of 8s to hit the target by imagining the appropriate hand movement, after which the trial terminates and the next one begins.

A Matlab process in the Presentation Machine receives the iEEG data from the Pegasus

Machine and preprocesses each data chunk using the same pipeline as in Stage 2. It later sends the preprocessed chunks to a second Matlab process that classifies these data chunks and streams the classification output as a LabStreamingLayer [17] stream. A third and final Matlab process connects to the LSL stream and moves the cursor 30 pixels to the right or left depending on the classification result. Code for all the stages is available on request.

Chapter 4

iEEG Motor Imagery Task: Relevant Feature Estimation

The iEEG BCI task described in the previous section was performed for 7 participants with 46 trials of left or right hand imagined movements. In order to get an estimate of the most relevant features for an online task, we performed an offline analysis, described in this section, of the data collected during the calibration stage. We first give a brief overview of the clinical profiles of the subjects involved in the study in section 4.1, followed by an analysis of the data collected during the calibration stage in section 4.2.

4.1 Subject description

The calibration data for the motor imagery task was collected from 7 subjects who were all patients undergoing treatment for intractable epilepsy, which included invasive monitoring to localize their seizures. Of the 7 subjects, 3 were female and the median age for the participants was 39 (see Table 4.1 for more details). An informed consent approved by the Institutional Review Board (IRB) at Carilion Hospital was obtained from the patients before performing the study. Adtech depth (hybrid) electrodes capable of recording Local Field Potentials (LFPs) and single unit activity were implanted for each subject and all the electrode positions were chosen solely for clinical purposes without considering our research

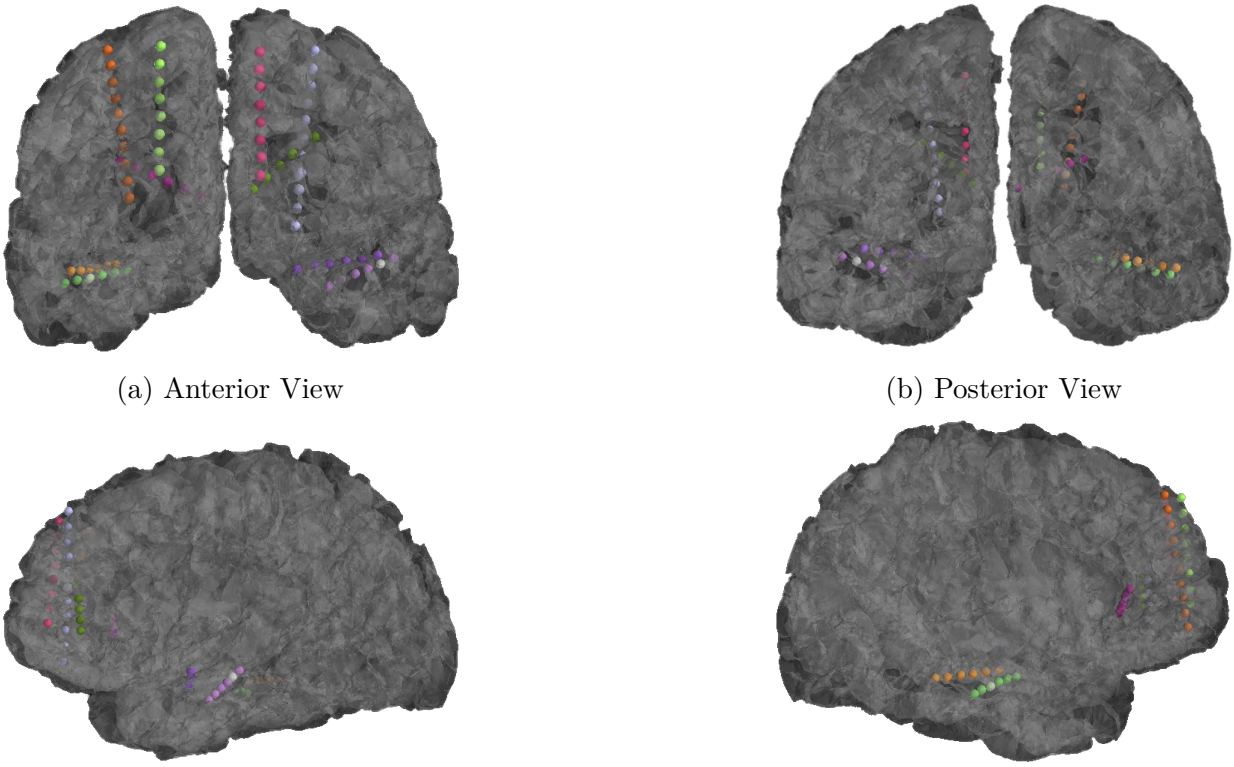

(a) Anterior View

(b) Posterior View

(c) Left Lateral View

(d) Right Lateral View

Figure 4.1: Electrode map of subject CAR 10. The colored dots indicate the location of the electrode contacts with the same color assigned to electrode contacts in the same depth electrode.

needs. The Micro-Macro depth electrodes had platinum contacts with a diameter of 1.3mm.

Fig. 4.1 shows the electrode map for subject CAR 10. All the electrodes used in the study are arranged in the form of linear strips where electrodes in the same strip are depicted using the same color. Each subject had about 200-250 electrodes implanted in either their temporal or frontal lobes, out of which 64 that did not shows signs of epileptic activity were chosen for the BCI experiment. Since the patients were under medication during their entire stay, and also because of their health conditions, we were allowed to conduct experiments only during a small window of time during a subject's stay. These difficulties along with the low number of patients who needed invasive monitoring allowed us to collect data from about 7 subjects during an entire year.

Subject	**Age**	**Gender**	**Dominant Hand**	**Epileptic region**
CAR04	24	F	R	L Temporal Lobe
CAR05	40	F	R	L Temporal Lobe
CAR07	57	M	R	L Temporal Lobe
CAR08	39	M	R	L Temporal/ L Hippocampal Lobe
CAR10	25	M	R	B/L Frontal
CAR11	39	F	R	L Frontal-temporal
CAR13	33	M	R	R Hippocampus

Table 4.1: Information regarding each of the 7 subjects involved in the intracranial EEG study

4.2 Feature Estimation

In this section, we analyze the intracranial EEG data obtained during the motor imagery task in order to find discriminatory features between left- and right-hand movements. Since

most of our electrode positions do not fall in the motor area of the brain, which has been well studied in previous work ([42], [6], [32]), we were interested in exploring the possibilities of the involvement of deep brain structures such as the amygdala, hippocampus, or the cingulate in motor-related tasks. We were particularly interested in the hippocampal electrodes and the temporal lobe in general, since recent studies ([9], [8]) have indicated its potential role in encoding and retrieving sequences of events that are involved in memories. Furthermore, all our subjects had electrodes that were in the hippocampus and other parts of the temporal lobe. Almost all of the previous work involving motor imagery looked at the spatial and spectral content in EEG or ECoG signals. These two recording modalities primarily provide signals from surface brain structures, while iEEG recordings provide us with the unique opportunity to examine the neural correlates of motor imagery in deep brain structures. We were also interested in studying the temporal nature of data across brain regions and also if there were any interactions between low- and high-frequency signals in brain structures during the motor task; such neural dynamics could potentially be leveraged as features to control BCI applications.

To find channels that were most discriminative during the motor imagery task, we first found the power difference between the left and right-hand imagined movements for all the channels from 3-200 Hz; this has been described in section 4.2.1. We later discuss our findings regarding high- and low-frequency interactions in the amygdala and the hippocampus in section 4.2.2.

4.2.1 Spatial and Spectral Features

To find channels that help distinguish between left- and right-hand movement tasks, we found the difference between the power of the signal envelope obtained from Hilbert Transform (we

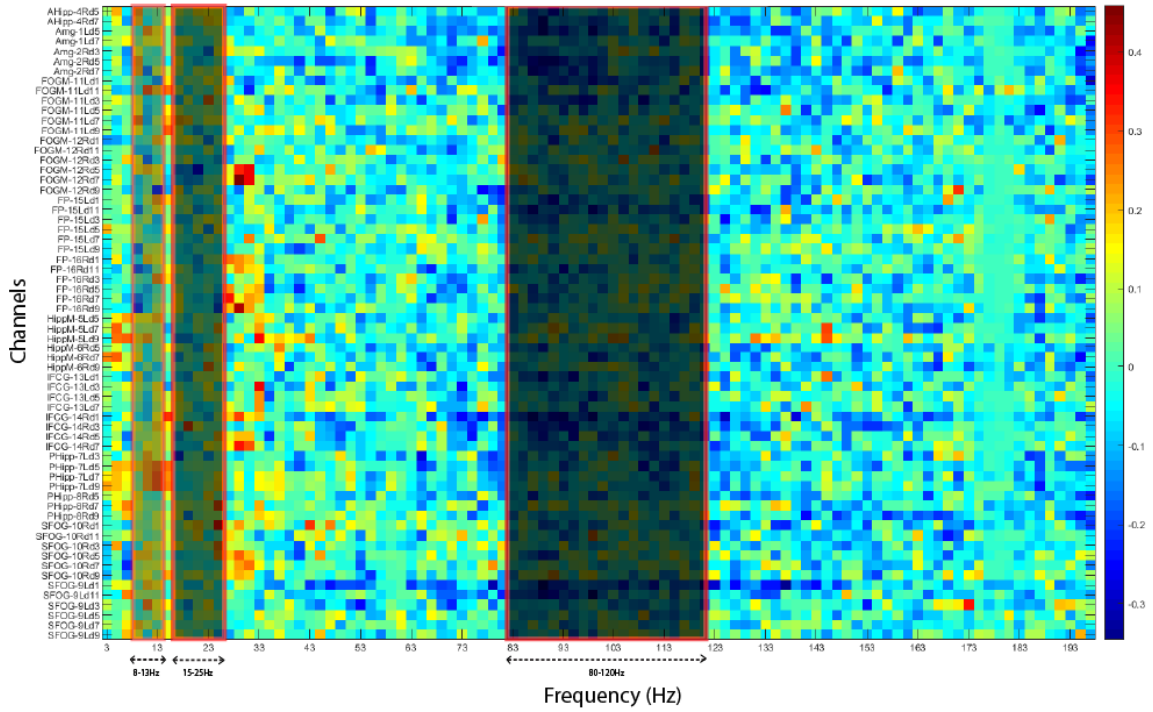

(a) Power difference between left- and right-hand movement as a function of frequency in all channels in subject CAR 04. The figure also shows the three selected frequency ranges of interest.

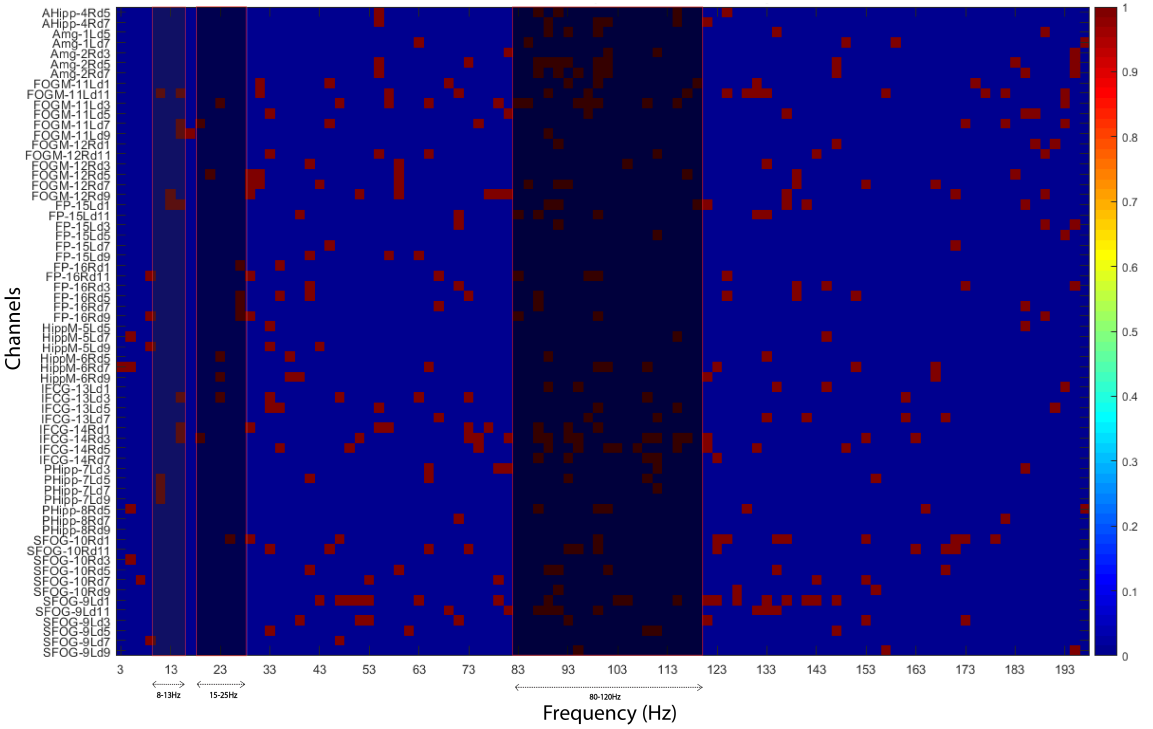

(b) Significant Power difference between left- and right-hand movements as a function of frequency in all channels in subject CAR 04. The red values indicate significant differences.

Figure 4.2: CAR 04 power and power significance plots

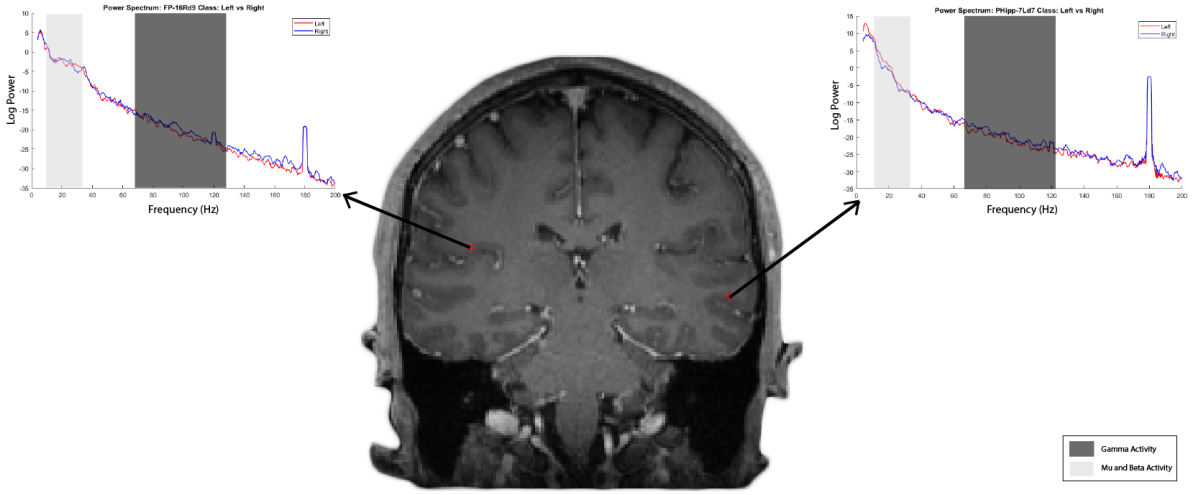

(a) Coronal view of subject CAR 04 showing the implanted electrodes (red markers) along with the power spectra for left- and right-hand movements at both electrodes.

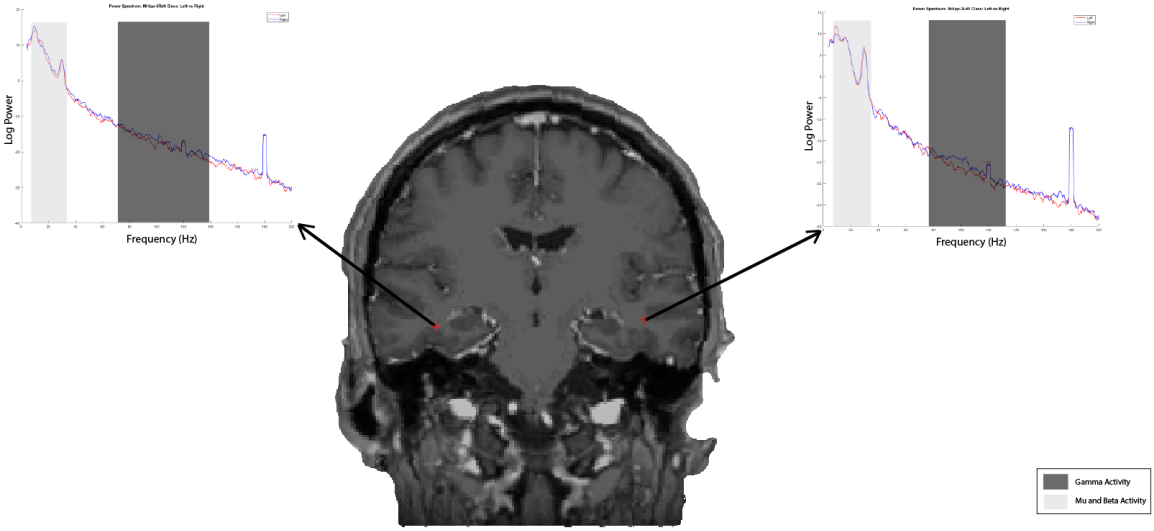

(b) Coronal view of subject CAR 10 showing the implanted electrodes (red markers) along with the power spectra for left- and right-hand movements at both electrodes

Figure 4.3: Power spectrum during left- and right-hand movements in both hemispheres for subjects CAR04 and CAR10

call this the power difference) for left and right movements in all frequencies from 3-200Hz for all channels. An example of this is shown in Fig. 4.2a for one of our subjects. We found the power difference by first finding the averaged power for each 2Hz bin from 3-300Hz for all the left and right trials (each trial was segmented at [-0.1, 2]s i.e., 0.1s before stimulus onset to 2s after stimulus onset) and then we found the difference in power between left and right trials across each frequency bin. Based on the power plots we segmented the plot into three frequency regions of interest: 8-13Hz, 15-25Hz, and 80-120Hz as shown in 4.2a. We later found channels that were significantly different during left and right trials after conducting a paired t-test of the signal powers for left and right movements. The significance plot is shown in Fig. 4.2b. The red values indicate the frequency bin at which the left vs right power is most significant and the blue regions indicate regions wherein the difference is not significant. Looking at Fig. 4.2a, it is clear that channels such as PHipp-7Ld3, PHipp-7Ld5, PHipp-7Ld7 and PHipp-7Ld9, which are in the left posterior hippocampus, have a higher left power when compared to right power at frequencies between 8-13Hz and 15-25Hz, whereas Phipp-8Rd5, Phipp-8Rd7, and Phipp-8Rd9, which are in the right posterior hippocampus, seem to have a lower left power when compared to right at the same frequencies. Signals from 8-13Hz known as the mu band and 15-25 Hz known as the beta band have been studied before in the motor areas and have been shown to produce Event Related Synchronizations (ERSs) and Event-Related Desynchronizations (ERDs) following actual or imagined hand movements ([37]). ERDs that occur in contralateral hemispheres at and around the mu and beta bands cause signal power to decrease as soon as the subject thinks about moving their hands followed by an increase in signal (ERS) after the hand movement.

Fig. 4.3a shows the coronal view of subject CAR 04 along with the power spectrum at two electrode locations, FP-16Rd9 and PHipp-7Ld7. These electrodes are in contralateral hemispheres. The electrode FP-16Rd9 has a lower power at frequencies around the mu-beta

bands during left-hand movements whereas electrode PHipp-7Ld7 has a lower power at the mu-beta bands during right-hand movements. Looking at the light grey regions on the power spectrum at PHipp-7Ld7, we can clearly see a decrease in power during right-hand movement along with an increase in power during right-hand movement at higher frequencies. A similar but opposite phenomenon can be observed in electrode FP-16Rd9, where we see a decrease in power at the low-frequency band (light gray region) during left-hand movement followed by an increase in power for right-hand movement at the high-frequency band (dark grey region). Fig. 4.3b shows a similar observation in subject CAR 10 (see Fig. 4.3b). These electrodes suggest that there is a lateralization of activity in temporal regions as seen in motor regions during imagined movements. This lateralization of power in the brain can be seen only in a small number of electrodes but is visible in all of the subjects; however, we were not able to consistently find these lateralizations in the same set of electrodes across all subjects. This might be because of problems such as the depth electrode strip not being located exactly in the region indicated by the label or some other biological phenomenon that hasn't been investigated yet. For these reasons we leave investigation of this phenomenon to future work.

4.2.2 Temporal Features

As discussed earlier, because of its role in sequential memory, a high difference in power between left and right-hand movement, and also because of its presence in all 7 subjects, we were interested in further analyzing the temporal signal characteristics in the hippocampus. We found that electrodes in the amygdala (present in 6 of the subjects) also showed a large power difference at lower and higher frequencies between left and right imagined movements. Because of these reasons we were interested in further analyzing the temporal signal characteristics in the amygdala and hippocampus electrodes; this analysis is described in this section.

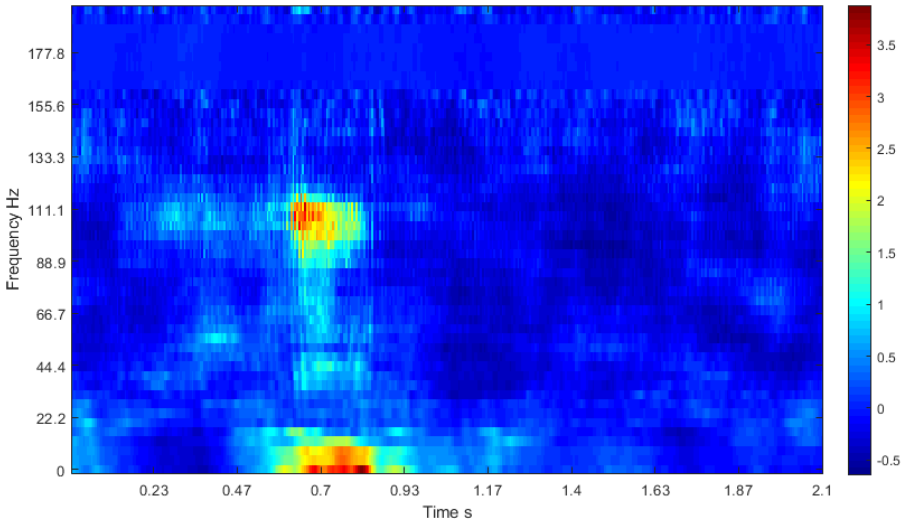

Figure 4.4: Spectrogram at one of the hippocampal electrodes in CAR04 showing the difference at both low and high frequencies between imagination of left- and right-hand movements.

Analyzing the spectrograms for the electrodes in these regions, we found there to be a large difference between left and right power at frequencies between 4-15Hz and 65-120Hz as seen in Fig. 4.4. This figure was constructed by averaging the signals from all the left trials and finding its spectrogram and finding the spectrogram of the averaged right trial signals at one of the hippocampal electrodes in subject CAR04, then taking the difference between the average right and left spectrograms. Prior to signal averaging across trials, we performed common averaging referencing (CAR, [25]) and mean subtraction in order to increase the signal to noise ratio and remove any low-frequency trends in data. After finding these differences in power, we were interested in knowing if the low and high-frequency components lagged or preceded one another, on average. We found the cross correlation between the low and high-frequency components in the hippocampus and amygdala in order to find the lag between these components. The average cross correlation was obtained by first selecting the amygdala and hippocampus electrodes that showed a significant power difference during left and right imagined movements and later finding the average cross

correlation across all these channels for all subjects between power in 3-15Hz and power in 65-115Hz. The average left and right cross correlation plots for all subjects are as shown in Fig. 4.5. This figure also shows the average cross correlation plot obtained after shuffling left and right class data with 10 repetitions across all trials but within each electrode; this plot acts as reference value indicating that all regions above it are significantly different.

Looking at the lags at the peak cross correlation values in left and right trials, we can see that, on average, the lag between the low- and high-frequency components during left movement is 0.27s, i.e, the high-frequency components lag behind the low-frequency components by 270ms. Also, the right trials had a lag of 0.0005s indicating that during right movements the high-frequency components occur on average at approximately the same time, with respect to neural time scales. It is therefore clear that there are cross correlation differences between low and high-frequency components during left and right trials.

In summary, we found a significant power difference in three frequency bins, 8-13Hz, 15-25Hz, and 80-120Hz, where the first two frequency bins in the mu and beta bands have been known to contribute during motor imagery tasks. We also found evidence of lateralization in some of the electrodes at the mu and beta bands, a phenomenon that has not been experimentally observed before in deep brain structures. The higher gamma band from 80-120Hz also seems to contain a number of significant channels, most of which belong to the amygdala and the hippocampus. These observations indicate that a classification algorithm that tries to learn discriminative features must focus on these frequency bands and channels in order to perform well. We also found there to be a latency of about 270 ms between lower and higher frequency bins during left-hand movement imagery and almost no latency during right-hand movement imagery. This suggests that temporal information might play a crucial role in a classification algorithm that performs well when classifying motor imagery data in intracranial EEG. In the next section, we discuss some of the classification algorithms

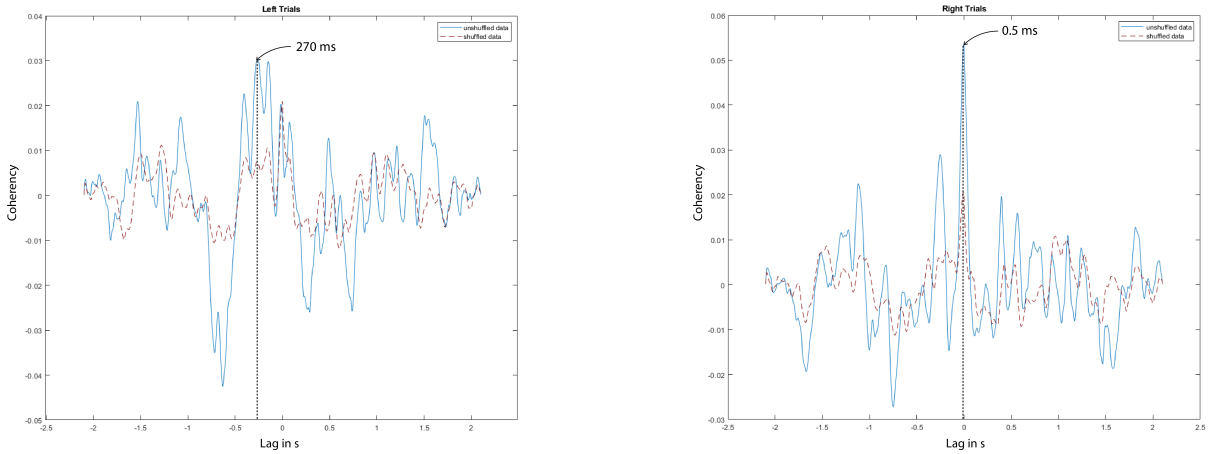

(a) Left trial cross correlation

(b) Right trial cross correlation

Figure 4.5: The average cross correlation between low and high frequency components during both left and right movements

used in oscillatory EEG signal classification and discuss their shortcomings when applied to intracranial EEG data.

Chapter 5

EEG Signal Classifiers

As described earlier, classifiers are used to map signals to the desired classes. This can be done either using classical machine learning techniques ([2], [46]) that generally require raw signals to be transformed into lower dimensional features or by using deep learning techniques ([19], [39]) that directly use minimally preprocessed signals. Most of the recent literature that has studied brain-computer interfaces using invasive signal collection techniques ([37], [22]) have used manual feature selection to find discriminative features which are later classified using a simple linear classifier. While this technique allows researchers to have control over the features being used to classify data, it might also prevent classification algorithms from finding new features not already employed in BCI tasks. With the limitations of different techniques in mind, in this section, we analyze 4 different EEG signal classification algorithms by applying them to an EEG motor imagery dataset and by comparing them with our new classification technique that is designed to use spectral, spatial and temporal features. Our main aim in the next two chapters will be to access the possibilities of using the current state of the art oscillatory EEG classification algorithms for classifying intracranial EEG data. We will also verify if the new classification technique performs better than the previous EEG classification techniques when applied to iEEG.

The remaining part of this chapter is organized as follows. In Sec. 5.1, we provide a brief overview of the different oscillatory EEG signal classification algorithms. Later in Sec. 5.3, we describe the motor imagery dataset and lastly, in Sec. 5.4, we discuss the classification

results and also the features learned by different classification algorithms.

5.1 Previous methods

5.1.1 Common Spatial Pattern

Common Spatial Pattern (CSP, [34], [25]) aims to learn a set of spatial filters that transform the high dimensional multichannel time series data into time-series that contains a lower number of channels. The spatial filters learned are such that data from two different classes are placed as far as possible in a low dimensional space. The spatial filters are found using a technique called simultaneous diagonalization of two covariance matrices which is as described in [34]. Usually, a set of m filters are extracted for each class and applied to the EEG data as shown below:

$$Z = WE \tag{5.1}$$

Where E is the input epoched EEG data containing N channels and T timesteps with shape NXT. And, W contains the $2m$ spatial filters (m filters of each class) each of shape $1XN$. Z is the output of shape mXT.

The log transform of each channel p in Z is then calculated using the equation below:

$$Z_p = log\left(\frac{var(Z_p)}{\sum_{i=1}^{2m} var(Z_p)}\right) \tag{5.2}$$

This reduces the dimensionality of the data to $mX1$. The output is then classified using a linear classifier such as Linear Discriminate Analysis (LDA, [27]). CSP used along with

a linear classifier has low computational requirements but is known to be susceptible to artifacts in the EEG data.

5.1.2 Filter Bank Common Spatial pattern

The Common Spatial Pattern (CSP) patterns described in the previous section required EEG data to be bandpass filtered between specific frequency bands and is prone to artifacts in the data. Filter Bank Common Spatial Pattern (FBCSP, [2]) was designed to overcome these shortcomings by allowing a feature selection algorithm to select features from required frequency bands. The FBCSP algorithm has four stages: a frequency filtering stage that filters the raw data into a number of bands, a spatial filter stage that applies CSP filters to signals from each of the frequency bins, a feature selection algorithm such as Mutual Information Based Best Individual Feature (MIBIF, [2]) that selects the most important CSP features and finally a classification stage that classifies the selected features using a classifier, for example by using a Support Vector Machine (SVM, [40]). FBCSP is more computationally intensive when compared to CSP, but, avoids manual frequency band selection.

5.1.3 Deep4Net

The authors in [39] implemented an end-to-end deep learning model (which we call Deep4net here) that is designed to learn a broad range of features from raw EEG data. Their 4 layers deep neural network is implemented using convolutions that learn spatial filters and temporal filters using 1D convolutions. By using techniques such as dropout [41], batch normalization [14] and an exponential linear activation function [7], they showed that their model could match FBCSP performance in motor imagery tasks.

5.1.4 EEGNet

The authors in [19] designed a CNN architecture that also matched the performance of FBCSP in motor imagery tasks but was able to do so using only a fraction of parameters as in Deep4Net. Their EEGNet architecture consists of 2 convolutional blocks, with the first block designed to learn bandpass filters along with spatial filters using 1D convolutionals. The second block used depthwise separable convolutions [5] designed to lower the parameter count while also acting as a regularizer. Batch normalization, exponential activations, and dropout were also included to avoid overfitting.

5.2 EphysNet

Both Deep4Net and EEGNet architectures were designed to learn spatial and spectral features from raw EEG data. In the Sec. 4.2.2 we showed that intracranial EEG data might also contain temporal information that could be leveraged by classification algorithms. To this end, we designed a new classification model known as EphysNet inspired from EEGNet that can learn spatial, spectral and temporal information. Fig. 5.1 shows the block diagram of EphysNet when applied to EEG signals. The model architecture is as follows:

- **Block 1**: This block consists of 8 1D convolutions that learn bandpass filtering of input data. The kernels used are one-fourth the length of each time series input. In our case since the input consists of 22 channels and 250 samples, this kernel has a size of 62. Batch Normalization is performed after the 1D convolution as indicated in 5.1.
- **Block 2**: Block 2 is designed using depth-wise separable convolutions [5] such that four features maps are learned using each of the 8 bandpass output feature maps. Separable convolutions as mentioned in [19] are used to reduce the number of parameters. It

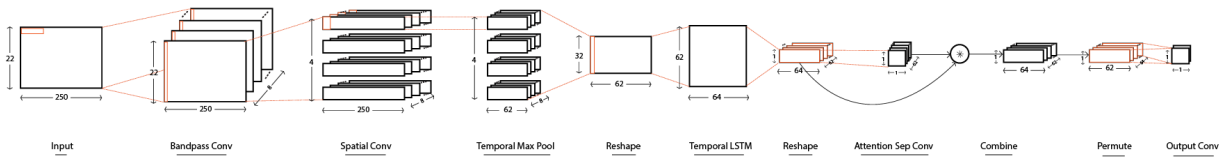

Figure 5.1: EphysNet Block Diagram used in EEG signal classification. Boxes in orange indicate the kernels applied at each stage.

also ensures that the network decouples learning from individual feature map using depth-wise convolutions to learning features from all features maps using point-wise convolutions. An Elu activation [7] function is applied after convolution.

- **Block 3**: Block 3 is designed to learn temporal features from the downsampled input data. It does this by first applying max pooling with a kernel size of (1, 4) in order to downsample the input data and to also reduce the parameter count. Later, it applies a one-directional LSTM with 64 units to learn 64 feature from each timestep. Dropout has been used in this block to prevent overfitting.

- **Block 4**: This block is used to learn a weight on each of the timestep such that the output layer and focus on features from desired timesteps. Inspiration for this layer comes from sequence2sequence networks with attention [4] that are designed to focus on the most important set of words in order to perform a language translation task.

- **Block 5**: This block applies the weights learned from block 4 to the output from block 3 in order to produce a weighted combination of the input. It also performs batch normalization to reduce overfitting.

- **Block 6**: This block uses a convolutional layer in place of the traditional dense later to learn a mapping from the input to the two desired classes.

Block	**Input Shape**	**Layer Name**	**Kernel Shape**	**Output Shape**	**Groups**
1	$BSX1X22X250$	Bandpass Convolution	$1X8X1X62$	$BSX8X22X250$	1
	$BSX8X22X250$	Bandpass Batch Norm	16	$BSX8X22X250$	
2	$BSX8X22X250$	Spatial Convolution	$8X32X22X1$	$BSX32X1X250$	8
	$BSX32X1X250$	Spatial Batch Norm	64	$BSX32X1X250$	
	$BSX32X1X250$	Elu		$BSX32X1X250$	
3	$BSX32X1X250$	Temporal Max Pool	$1X4$	$BSX32X1X62$	
	$BSX32X1X62$	Temporal Dropout(p=0.5)		$BSX32X1X62$	
	$BSX32X1X62$	Reshape		$BSX32X62$	
	$BSX32X62$	Permute		$BSX62X32$	
	$BSX62X32$	Temporal (one directional LSTM)	64 units	$BSX62X64$	
	$BSX62X64$	Reshape		$BSX62X64X1$	
4	$BSX62X64X1$	Attention Depth	$62X1X64X1$	$BSX62X1X1$	62
	$BSX62X1X1$	Attention Point	$62X62X1X1$	$BSX62X1X1$	1
	$BSX62X1X1$	Softmax		$BSX62X1X1$	
5	$BSX62X64X1$ & $BSX62X1X1$	Combine output from 3 and 4		$BSX62X64X1$	
	$BSX62X64X1$	Permute		$BSX64X62X1$	
	$BSX62X64X1$	Batch Norm	128	$BSX64X62X1$	
6	$BSX64X62X1$	Output Convolution	$64X2X62X1$	$BSX2X1X1$	
	$BSX2X1X1$	Reshape		$BSX2$	
	$BSX2$	Softmax		$BSX2$	

Table 5.1: EphysNet Model Architecture. BS is the batch size

Model	# Parameters
Deep4Net	77677
EEGNet	1666
EphysNet	42246

Table 5.2: Number of model parameters when using Deep4Net, EEGNet and EphysNet on EEG motor imagery data

5.3 EEG dataset description and experimental setup

The EEG data used to compare different classification algorithms on the motor imagery task comes from BCI Competition IV Dataset 2a [43]. This EEG dataset comes from 9 subjects performing 4 motor imagery tasks (left hand, right hand, both feet and tongue movement). EEG data from 22 channels were recorded during two sessions each containing 288 trials. The first session is used as a training dataset and the second session is used for evaluation purposes. We segmented the data from 0.5s prior to stimulus onset to 4s after stimulus onset and bandpass filtered the data from 4-100Hz using a zero phase Butterworth filter of 3rd order. Then we removed the feet and tongue movement trials from the dataset and chunked each trial into segments of 1s with an overlap of 32ms. We decided to chunk the data to simulate a real BCI experiment that usually employs data in similar chunk sizes and to also increase the amount of training data. We performed a 10 fold cross-validation on the training set and tested the model on session 2 data. All the deep learning classifiers used Adam [16] optimizer implemented in PyTorch along with an exponential learning rate decay during training. The classifiers were constructed using PyTorch [31] with the data preprocessing done using python MNE [11]. We trained the model on a Nvidia P100 GPU using the resources provided by the Advanced Research Computing facility at Virginia Tech. Code for all the classifiers is available upon request.

5.4 EEG Motor Imagery Classification Results

We compared the different models discussed earlier on the BCI competition dataset in the 2 hand motor imagery task. Table 5.3 gives the test accuracy for all the 9 subjects using each of the classifiers. EphysNet performs significantly better than the other classifiers for subjects

Subject	CSP	FBCSP	Deep4Net	EEGNet	EphysNet
1	70.378788 +- 1.218932	77.209596+- 2.152676	77.470328 +- 2.550946	77.664141 +- 1.610556	78.256944 +- 1.300614
2	50.991162 +- 2.345170	53.440657 +- 1.323572	52.742424 +- 1.596811	50.440657 +- 1.257790	52.996212 +- 5.516928
3	82.897727 +- 1.572094	79.905303 +- 1.293841	83.805556 +- 1.725818	84.193813 +- 3.250810	**87.450758 +- 1.509868**
4	60.372475 +- 2.384240	58.554293 +- 1.667263	62.167929 +- 2.996915	63.636995 +- 0.932932	62.172348 +- 2.685307
5	50.227273 +- 3.098911	69.223485 +- 2.512551	51.094697 +- 1.677938	63.332071 +- 9.719778	52.393939 +- 2.844675
6	56.351010 +- 2.989147	59.949495 +- 1.572357	61.439394 +- 1.526376	61.435606 +- 0.902708	60.188131 +- 1.644080
7	53.453283 +- 1.876437	76.710859 +- 2.176514	74.499369 +- 2.511697	**76.723485 +- 1.650654**	74.212753 +- 1.974648
8	84.040404 +- 1.734211	77.683081 +- 1.861349	83.267045 +- 1.472639	84.868687 +- 0.904814	**85.606692 +- 0.847031**
9	77.222222 +- 1.452725	77.689394 +- 1.162437	76.990530 +- 1.375153	75.379419 +- 2.446994	75.481692 +- 2.792262

Table 5.3: Test Accuracy along with the standard deviation after training CSP, FBCSP, Deep4Net, EEGNet and EphysNet on all the 9 EEG subjects. The values highlighted indicates a significantly higher ($p<0.05$) test accuracy when compared to the other classifiers

3 and 8 whereas EEGNet performs better for subject 7. For the remaining six subjects there was no significant difference in performance among the classifiers. This table shows that EphysNet was able to learn features from subjects that already had high classification results using the other classifiers. This indicates that incorporation of temporal information into a classifier that is already performing relatively well for a given subject may result in further improvement. In order to gain insights into why EphysNet performed well we examined the features extracted by EphysNet.

5.5 Feature Visualization

To get an understanding of the features learned by EphysNet and to also verify that the features being used to classify signals are from neural signals and not artifacts in the data, we explored three different feature visualization techniques in this section:

- **Visualizing Bandpass Convolutional Kernels**: Artifacts present in EEG data are usually Electromyographic (EMG) or Electrooculographic (EOG) signals that result from muscle or eye movements. Since in BCIs we are only interested in producing

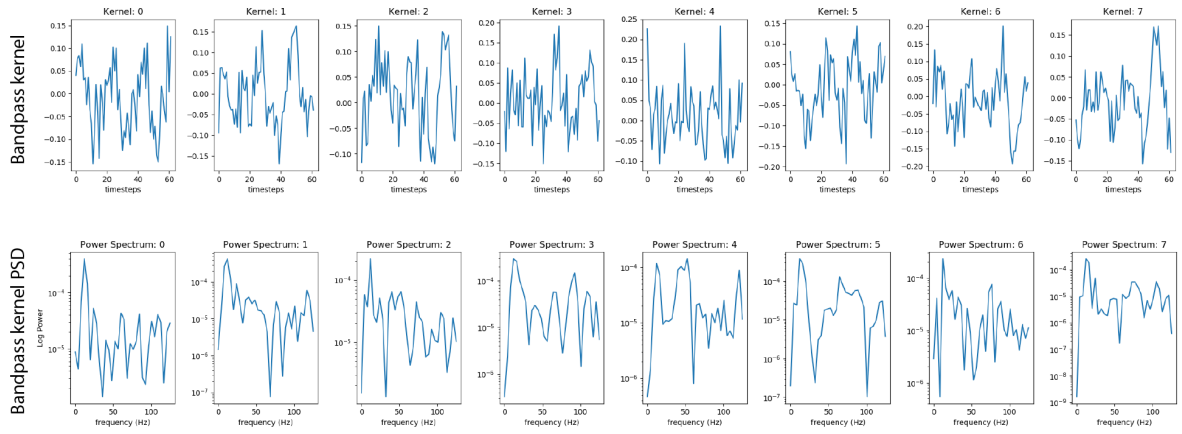

Figure 5.2: Visualizing Bandpass Convolutional Kernels: Top row represents the bandpass kernels learnt by EphyNet and the bottom row represents the power spectral density of the kernel above it for subject 3 during 2 hand motor imagery

control signals using brain wave activity and not EMG or EOG artifacts, we visualized the bandpass kernel learned by EphysNet for subject 3 as shown in Fig. 5.2 and analyzed the power spectral density of the kernels learned. Looking at the power spectral density it can clearly be seen that the peak of most of the kernels is around 12Hz which belongs to the mu band (signals in this band are known for their ERS and ERD characteristics discussed earlier). We also see that both the frequency components lower than 8Hz and around 60Hz are not given much weight by the classifier.

- **Visualizing Spectral Filters**: We know that during motor imagery tasks ERD occurs in the contralateral hemispheres of the brain near the motor cortex [46]. In Fig. 5.2, we have visualized the 4 spatial filters learned by each of the first four bandpass filters for subject 3. Ignoring the extrapolation errors in the spatial topological plot, we see that the spatial filters have either a low or high magnitude value at electrodes near the motor cortex.

- **SHAP based feature visualization**: SHAP (SHapley Additive exPlanations) [26] is

designed to assign each feature in the input with a numerical value that indicates the importance of a feature during each classification category. We used SHAP in order to find the important features during each of the classes and to also verify if the features learned were near the contralateral motor area. Fig. 5.4 shows the raw EEG signals represented as an image along with the importance values assigned by SHAP towards its right. From the topological plots of average importance values during the hand movements, it is clear that the model has, in fact, placed importance on the signals from the contralateral side of the imagined movement. Furthermore, the signals given importance are mostly located near the motor region. Since we trained EphysNet using overlapping chunks of data, we were also interested in whether the model learned to recognize features from different time points. We passed the right trial chunks with an overlap of 32ms from [0.5, 2]s and found the corresponding features at each chunk. Fig. 5.5 shows the right trials in the left column along with their right SHAP values in the right column. We can clearly see the chunk of importance values moves from the right of the chunk to the left, as the chunk moves forward in time. This figure includes that our model has in fact learned to track importance features through time.

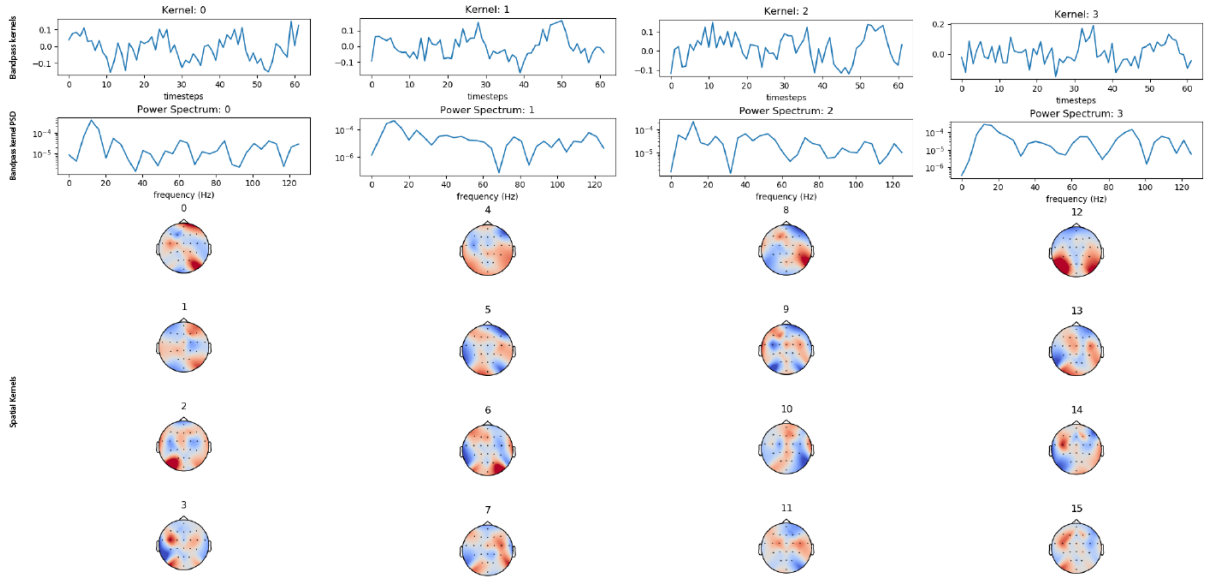

Figure 5.3: Visualizing Spectral Filters: Top row shows the first 4 bandpass kernels learnt by EphysNet o subject 3. The second row shows the power spectral density of the kernels above it. The last four rows show the spatial filters learnt using each of the bandpass filters above it.

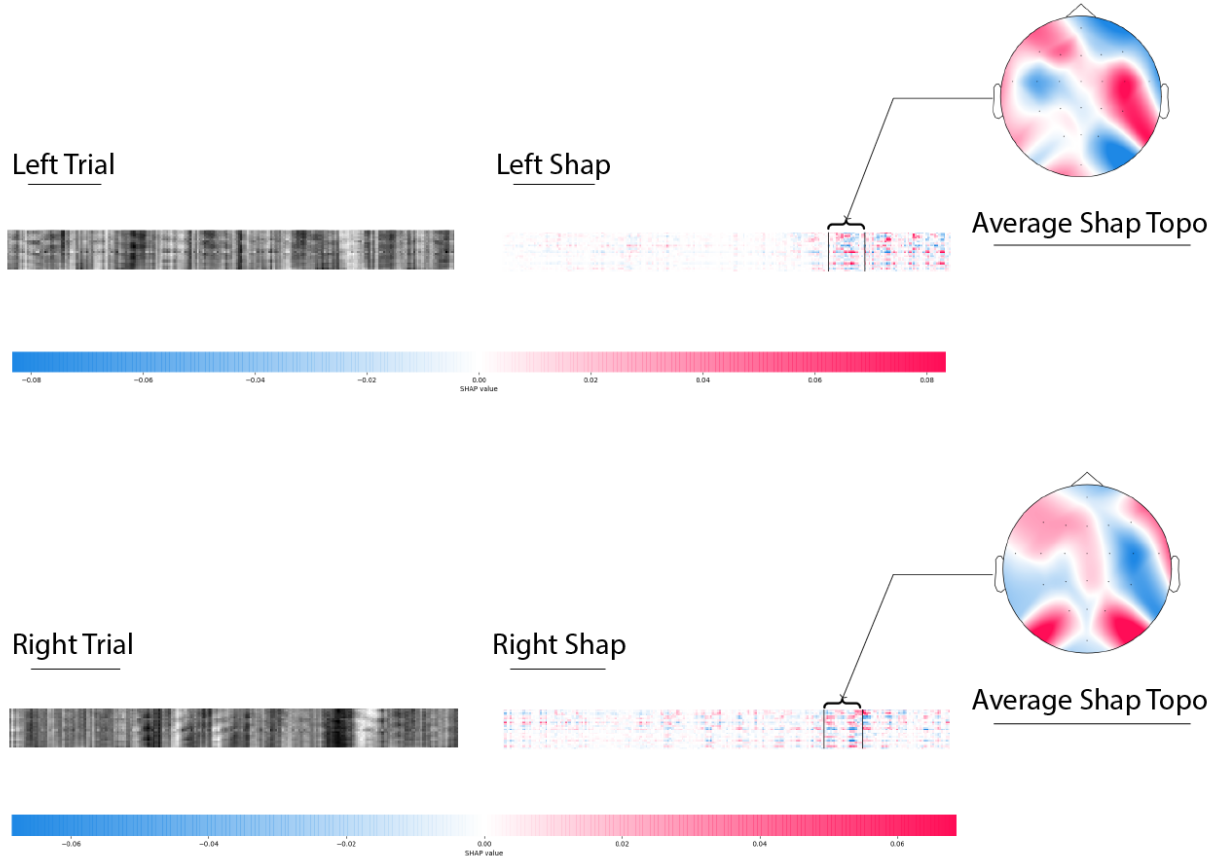

Figure 5.4: SHAP based feature visualization: Top row shows the raw signals at all channels for subject 3 during left hand movement along with its importance values towards its right. The topoplot consists of the average of importance values assigned during the left hand movement time samples. Bottom row indicates the same thing but for the right trials. Both the left and right trials are 1s segments from [-0.5, 0.5]s

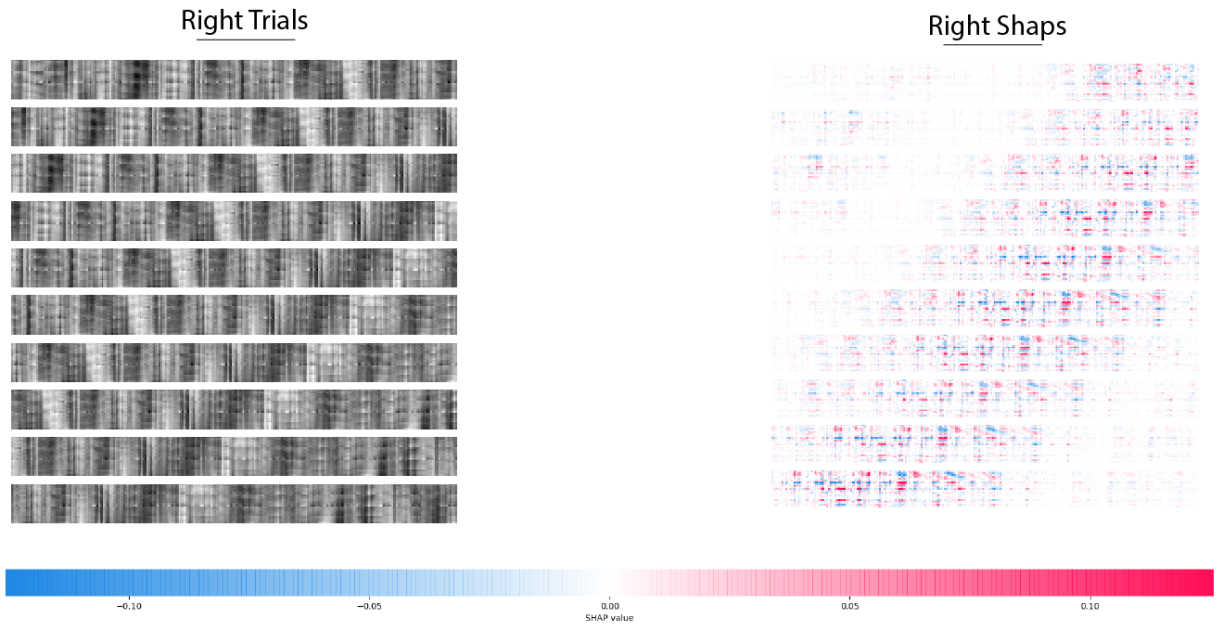

Figure 5.5: SHAP based feature visualization to track features: Left Column shows the raw eeg traces along a continuous set of data 1s long data chunks. The right column shows the SHAP values of the chunks towards their left.The signal moves forward in time as we proceed from the top to the bottom row.

Chapter 6

iEEG Signal Classifiers

In this chapter, we apply the classification algorithms discussed in the previous chapter to the intracranial EEG data obtained during the two hand motor imagery task described earlier. In Sec. 6.1, we give an overview of the modifications made to the five classification algorithms when used in iEEG data and also discuss the data processing done to the iEEG data. In Sec. 6.2, we discuss the classification results on the motor imagery task followed by feature visualization of EphysNet in Sec. 6.3.

6.1 Experimental Setup

Since it is known that high-frequency signals contain ([21], [20]) information that might be very useful in order to distinguish motor imagery tasks, we decided to allow the classifiers to be able to learn frequency components up to 256Hz by downsampling the original 2KHz signal. Downsampling the signal not only preserves known high-frequency components but also

Model	# Parameters
Deep4Net	105927
EEGNet	3154
EphysNet	69330

Table 6.1: Number of model parameters when using Deep4Net, EEGNet and EphysNet on iEEG motor imagery data

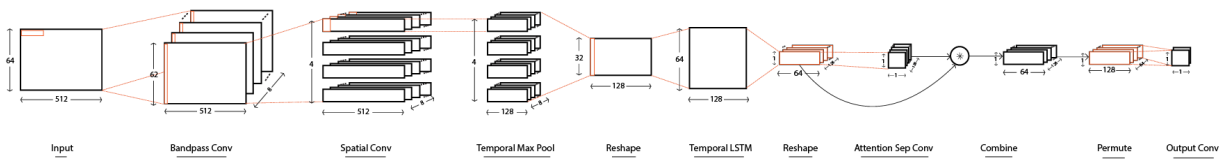

Figure 6.1: EphysNet when applied to iEEG data. The sizes of feature map after each layer is indicatd along with the kernel shapes used in each layer with orange boxes.

Block	**Input Shape**	**Layer Name**	**Kernel Shape**	**Output Shape**	**Groups**
1	$BSX1X64X512$	Bandpass Convolution	$1X8X1X128$	$BSX8X64X512$	1
	$BSX8X64X512$	Bandpass Batch Norm	16	$BSX8X64X512$	
2	$BSX8X64X512$	Spatial Convolution	$8X32X64X1$	$BSX32X1X512$	8
	$BSX32X1X512$	Spatial Batch Norm	64	$BSX32X1X512$	
	$BSX32X1X512$	Elu		$BSX32X1X512$	
	$BSX32X1X512$	Temporal Max Pool	$1X4$	$BSX32X1X128$	
	$BSX32X1X128$	Temporal Dropout(p=0.5)		$BSX32X1X128$	
	$BSX32X1X128$	Reshape		$BSX32X128$	
	$BSX32X128$	Permute		$BSX128X32$	
3	$BSX128X32$	Temporal (one directional LSTM)	64 units	$BSX128X64$	
	$BSX128X64$	Reshape		$BSX128X64X1$	
4	$BSX128X64X1$	Attention Depth	$128X1X64X1$	$BSX128X1X1$	128
	$BSX128X1X1$	Attention Point	$128X128X1X1$	$BSX128X1X1$	1
	$BSX128X1X1$	Softmax		$BSX128X1X1$	
5	$BSX128X64X1$ & $BSX128X1X1$	Combine output from 3 and 4		$BSX128X64X1$	
	$BSX128X64X1$	Permute		$BSX64X128X1$	
	$BSX128X64X1$	Batch Norm	128	$BSX64X128X1$	
6	$BSX64X128X1$	Output Convolution	$64X2X128X1$	$BSX2X1X1$	
	$BSX2X1X1$	Reshape		$BSX2$	
	$BSX2$	Softmax		$BSX2$	

Table 6.2: EphysNet Model Architecture. BS is the batch size

Subject	CSP	Deep4Net	EEGNet	EphysNet
CAR04	50.875000 +- 11.929917	63.645000 +- 8.229078	69.625000 +- 9.168049	62.900000 +- 10.093438
CAR05	65.707071 +- 10.551003	66.130000 +- 7.409494	64.875000 +- 10.400270	61.025000 +- 7.689644
CAR07	48.300000 +- 6.100774	69.395000 +- 5.500020	60.475000 +- 12.146219	73.325000 +- 2.522524
CAR08	49.525000 +- 12.425584	**92.970000 +- 7.983364**	82.950000 +- 14.465390	79.975000 +- 10.547186
CAR10	62.929293 +- 4.456989	55.920000 +- 8.968478	57.150000 +- 14.376283	52.975000 +- 9.226626
CAR11	54.696970 +- 6.870667	57.080000 +- 10.493741	46.225000 +- 14.072335	49.950000 +- 9.597395
CAR13	45.375000 +- 15.057413	66.104286 +- 5.904820	54.025000 +- 5.506190	55.275000 +- 6.231422

Table 6.3: Test Accuracies after 10 repeats on four classifiers when applied to iEEG Motor Imagery Task. FBCSP is excluded from analysis as it was not possible to increase its classification accuracy beyond chance on any of the subjects. Bold values indicates stastically significant results ($p<0.05$)

reduces the number of parameters in the model thereby reducing the chances of overfitting. We also performed CAR and mean subtraction to the data in order to increase the signal to noise ratio. Because of the increased signal timesteps from 250 to 512 and an increase in the number of channels from 22 to 64, the iEEG classifiers had a slight increase in the number of model parameters when compared to its EEG counter-part (see Table 6.1 and 5.2). Increases in kernel sizes for EEGNet and Deep4Net were performed according to the information provided by their respective authors. Fig. 6.1 shows the feature map sizes after each layer in the EphysNet. Comparing this to Fig. 5.1, we clearly see how the increase in the number of channels and timesteps dictates the increase in kernel sizes and feature map sizes. See Table. 6.2 in order to get a detailed overview of the feature map sizes along with the respective kernels.

6.2 iEEG Motor Imagery Classification Results

We trained each of the five classifiers on the iEEG dataset collected while subjects performed the two hand motor imagery task. Each subject performed a total of 46 trials during the

calibration stage (stage 1) each lasting 4s, out of which 2 random left and right trials were used as testing data and the remaining 42 trials where used as training (90%) and validation (10%) data. After segmenting each trial from [-0.5, 4]s and chunking them into 1s overlapping segments, each trial produced 100 chunks per segment. We repeated the experiment 10 times, selecting 2 random left and right trials as testing each time and training/validating on the rest. The classification results for all the classifiers expect FBCSP is as shown in Table. 6.3. FBCSP was excluded from analysis for iEEG as it was not possible to increase its test accuracy beyond change (50%). From Table 6.3, we can see Deep4Net on subject CAR08 produced statistically significant results and that CSP classifier performed the worst in subjects CAR07, CAR08 and CAR13. This is expected as, CSP is known to produce bad results in the presence of noise in the data [2], and also because it has to learn from a broad frequency range (4-200Hz) when used in iEEG. Deep4Net, EEGNet, and EphysNet seems to perform comparably on all the subjects. When compared to the classification results obtained using the EEG data, we can clearly see that iEEG data produces lower classification results. This might be because of the larger number of channels, the higher sampling rate designed to capture high-frequency information when compared to EEGs and also the fact that in motor imagery tasks using EEG, the electrode locations were in the motor cortex, where as, iEEG does not have any electrodes in the motor cortex. The test accuracy values also have a higher standard deviation in iEEG when compared to EEG because we only used 4 trials for testing and so if a subject performed poorly on any one of those trials the classification results will be poor. Collecting another session of data only for testing might allow for a better comparison between the performance on EEG data versus iEEG data.

6.3 Feature Visualization

Similar to Sec. 5.5 in this section, we look at the temporal kernels, SHAP values during left and right trials and the SHAP features over time in order to get an understanding of the features learned by EphysNet.

- **Visualizing Bandpass Convolutional Kernels**: Fig. 6.2 shows the bandpass kernels along with the power spectral density of the kernels. Looking at the peaks in the power spectral density, we observe that activity around 100Hz is captured by kernels 2 and 6 whereas kernels 1, 2 and 4 mainly capture lower frequency activity from 20-70Hz. Based on the offline analysis done earlier, we found there to be high-frequency activity around 80-120Hz and also around 15-26Hz. We do in fact see some signals in these frequency bands being learned by the filters, we do not, however, observe a high power in the mu band.

- **SHAP based feature visualization**: Fig. 6.3 shows the raw left and right trials along with their SHAP values for subject CAR08. We selected a time window that represents the instance when the subject imagined moving their arms and took the average of the SHAP values during that time period as indicated in the Average SHAP plot. Looking the left average SHAP plot, we see that electrodes AHipp-3Ld6, Amg-1Ld5 and Amg-2Rd2 contributed during the left movement and from the right average SHAP plot the LSFG-9L strip seems to contain high SHAP values. From Hilbert Power difference in Fig. A.2, we see that some channels in the Hippocampus and Amygdala along with the LSFG-9L strip had significant differences in power during left and right-hand movement. In order to determine if the features learned to distinguish between left and right movement are being tracked during each of the signal chunks, we plotted 10 consecutive signal chunks along with their SHAP values in Fig. 6.4. Similar to

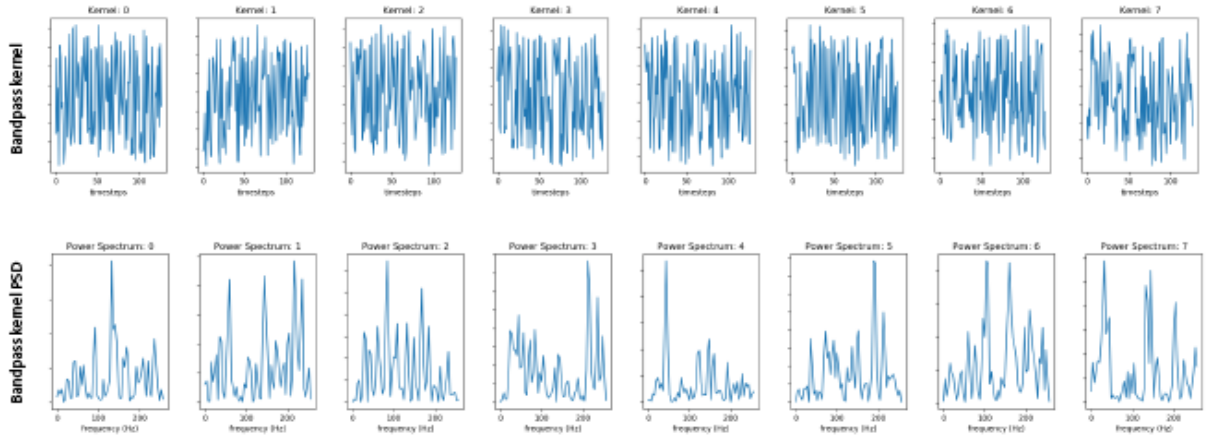

Figure 6.2: Visualizing Bandpass Convolutional Kernels: The top row shows the raw bandpass kernel values learnt by EPhysNet along with its power spectral density in the bottom row.

EEG results, we again see that the classifiers were able to track the required features in time.

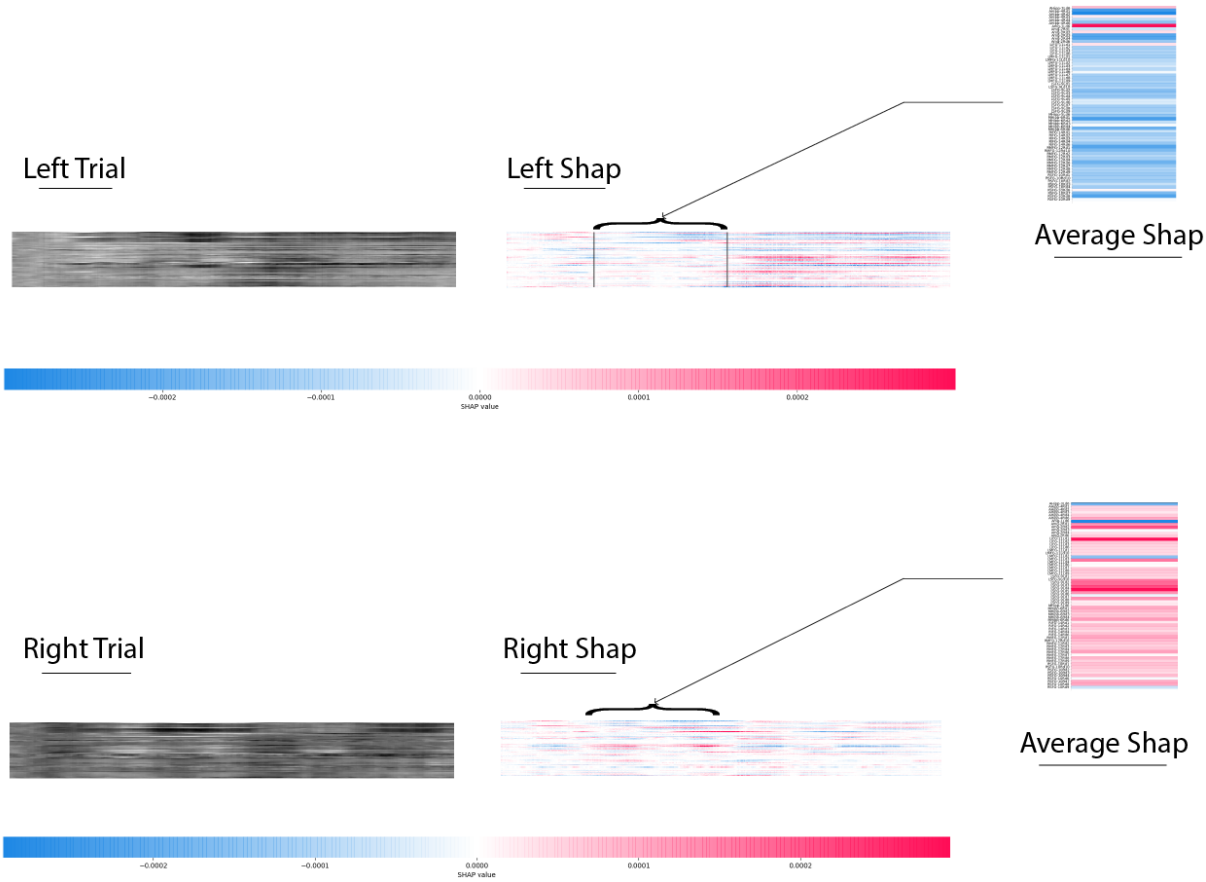

Figure 6.3: SHAP based feature visualization: Top row shows the raw iEEG data along all the 64 channels from [-0.1, 0.9]s during the left trial as an image along with its corresponding SHAP values towards its right. The Average SHAP values in movement window in shown towards the extreme right. Bottom row depicts a similar observatino during the right trial. The iEEG channels are visible when zooming in on the digital version.

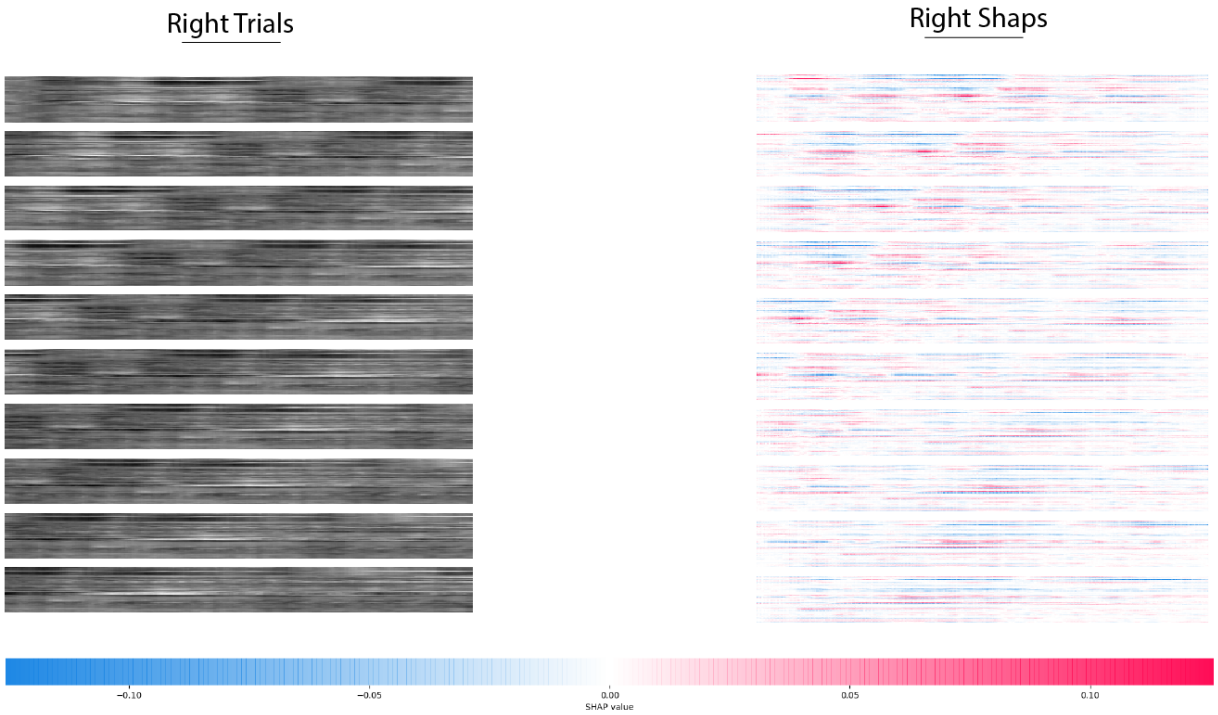

Figure 6.4: SHAP based feature visualization: Left column shows 10 consecutive (top to bottom) raw iEEG traces as image and the right column shows its corresponding SHAP values. All chunks were obtained during right hand movement from subject CAR08.

Chapter 7

Conclusions and Future Work

With the final goal of developing a classifier and analyzing its performance on intracranial EEG, in this work, we started off by designing a robust iEEG data acquisition and signal processing pipeline. We implemented the data acquisition pipeline using MATLAB with the added ability to use a classifier from Python. We also discussed the BCI experimental paradigm used to collect our iEEG data along with the preprocessing done. We later analyzed the iEEG data obtained from the two hand motor imagery task from 7 subjects in order to find relevant spectral, spatial and temporal features manually. Looking at the power difference between left and right-hand movements, we found there to be a large number of significant frequency bins that differed in power at three major frequency bands. Two of these bands were also found to include the mu and beta band that is known to play a role during motor movements. Inspired by the fact that the hippocampal electrodes are involved in processing sequential memory and also because the hippocampal and amygdala electrodes were present in 6 of the 7 subjects, we further showed there to be a time lag in the high (65-115Hz) and low (3-15Hz) frequency signals during imagined left hand movement and that this lag was absent during imagined right movement.

Using the results from this offline data analysis, we hypothesized that a good classification algorithm must learn these features in order to perform well in an online task. To this end, we designed EphysNet, a classification algorithm that learns to automatically extract spatial, spectral and temporal information from electrophysiological data. We tested this

classification algorithm on EEG motor imagery data and also compared it to other classifiers. We found there to be a significant performance increase when using our classifier on subjects that performed well during the calibration stage. Feature visualization was performed on EphysNet when used on EEG data and we found the classifier to use frequency components in the mu and beta band from contralateral electrodes in the motor region of the brain. We finally compared the performance of EphsyNet along with several other classifiers on the two hand iEEG motor imagery dataset and found there to be so significant difference between Conv4Net, EEGNet, and EphysNet except in subject CAR08, where Deep4Net seemed to perform better. We later performed feature visualization on EphysNet when used on iEEG and found spatial filters that agreed with power difference between the left-right power difference and also found that the bandpass filters had mainly learned to used frequency components around 100Hz and from 2–70Hz. These findings clearly show the potential of using end-to-end classification algorithms on electrophysiological data as they do not any manual feature selection to be done, they also require minimal data preprocessing and have a low number of parameters thereby allowing them to be used in online tasks.

Comparing the classification results on the two hand EEG and iEEG datasets, we clearly see that the EEG task seems to perform better on average. This might be because the subjects used in the EEG experiments might have a better mental health condition, not subjected to constant medication and worry about seizures. Also, because the electrodes used in the EEG experiment come from the motor cortex which has well studied previously, but, the depth electrodes used in our case are not in the motor cortex. Also, because of the lower number of test samples available during iEEG classification, its test accuracy had a higher variance when compared to the EEG classifiers. An entire session dedicated to collecting only test samples would give us a better estimation of the classifiers abilities on iEEG data.

Bibliography

[1] Kai Keng Ang et al. "Clinical study of neurorehabilitation in stroke using EEG-based motor imagery brain-computer interface with robotic feedback". In: *2010 Annual International Conference of the IEEE Engineering in Medicine and Biology*. IEEE. 2010, pp. 5549–5552.

[2] Kai Keng Ang et al. "Filter bank common spatial pattern (FBCSP) in brain-computer interface". In: *2008 IEEE International Joint Conference on Neural Networks (IEEE World Congress on Computational Intelligence)*. IEEE. 2008, pp. 2390–2397.

[3] Andreas Antoniades et al. "Deep learning for epileptic intracranial EEG data". In: *2016 IEEE 26th International Workshop on Machine Learning for Signal Processing (MLSP)*. IEEE. 2016, pp. 1–6.

[4] Dzmitry Bahdanau, Kyunghyun Cho, and Yoshua Bengio. "Neural machine translation by jointly learning to align and translate". In: *arXiv preprint arXiv:1409.0473* (2014).

[5] François Chollet. "Xception: Deep learning with depthwise separable convolutions". In: *Proceedings of the IEEE conference on computer vision and pattern recognition*. 2017, pp. 1251–1258.

[6] Febo Cincotti et al. "Non-invasive brain–computer interface system: towards its application as assistive technology". In: *Brain research bulletin* 75.6 (2008), pp. 796–803.

[7] Djork-Arné Clevert, Thomas Unterthiner, and Sepp Hochreiter. "Fast and accurate deep network learning by exponential linear units (elus)". In: *arXiv preprint arXiv:1511.07289* (2015).

[8] Loren M DeVito and Howard Eichenbaum. “Memory for the order of events in specific sequences: contributions of the hippocampus and medial prefrontal cortex”. In: *Journal of Neuroscience* 31.9 (2011), pp. 3169–3175.

[9] Norbert J Fortin, Kara L Agster, and Howard B Eichenbaum. “Critical role of the hippocampus in memory for sequences of events”. In: *Nature neuroscience* 5.5 (2002), p. 458.

[10] William J Gehring et al. “The error-related negativity”. In: *Perspectives on Psychological Science* 13.2 (2018), pp. 200–204.

[11] Alexandre Gramfort et al. “MNE software for processing MEG and EEG data”. In: *Neuroimage* 86 (2014), pp. 446–460.

[12] Cuntai Guan, Manoj Thulasidas, and Jiankang Wu. “High performance P300 speller for brain-computer interface”. In: *IEEE International Workshop on Biomedical Circuits and Systems, 2004.* IEEE. 2004, S3–5.

[13] Leigh R Hochberg et al. “Reach and grasp by people with tetraplegia using a neurally controlled robotic arm”. In: *Nature* 485.7398 (2012), p. 372.

[14] Sergey Ioffe and Christian Szegedy. “Batch normalization: Accelerating deep network training by reducing internal covariate shift”. In: *arXiv preprint arXiv:1502.03167* (2015).

[15] Christopher L Jones et al. “Design and development of the cable actuated finger exoskeleton for hand rehabilitation following stroke”. In: *IEEE/ASME Transactions on Mechatronics* 19.1 (2014), pp. 131–140.

[16] Diederik P Kingma and Jimmy Ba. “Adam: A method for stochastic optimization”. In: *arXiv preprint arXiv:1412.6980* (2014).

[17] C Kothe. “Lab streaming layer (LSL)”. In: *https://github. com/sccn/labstreaminglayer. Accessed on October* 26 (2014), p. 2015.

[18] Karl LaFleur et al. “Quadcopter control in three-dimensional space using a noninvasive motor imagery-based brain–computer interface”. In: *Journal of neural engineering* 10.4 (2013), p. 046003.

[19] Vernon Lawhern et al. “EEGNet: A Compact Convolutional Network for EEG-based Brain-Computer Interfaces”. In: *Journal of neural engineering* 15 5 (2018), p. 056013.

[20] Eric C Leuthardt et al. “A brain-computer interface using electrocorticographic signals in humans”. In: *Journal of neural engineering* 1.2 (2004), p. 63.

[21] Eric C Leuthardt et al. “Electrocorticography-based brain computer interface-the Seattle experience”. In: *IEEE Transactions on Neural Systems and Rehabilitation Engineering* 14.2 (2006), pp. 194–198.

[22] Simon P Levine et al. “Identification of electrocorticogram patterns as the basis for a direct brain interface”. In: *Journal of clinical neurophysiology* 16.5 (1999), p. 439.

[23] Lun-De Liao et al. “Gaming control using a wearable and wireless EEG-based brain-computer interface device with novel dry foam-based sensors”. In: *Journal of neuroengineering and rehabilitation* 9.1 (2012), p. 5.

[24] Chin-Teng Lin et al. “Brain computer interface-based smart living environmental auto-adjustment control system in UPnP home networking”. In: *IEEE Systems Journal* 8.2 (2014), pp. 363–370.

[25] Kip A Ludwig et al. “Using a common average reference to improve cortical neuron recordings from microelectrode arrays”. In: *Journal of neurophysiology* 101.3 (2009), pp. 1679–1689.

[26] Scott M Lundberg and Su-In Lee. "A unified approach to interpreting model predictions". In: *Advances in Neural Information Processing Systems*. 2017, pp. 4765–4774.

[27] Sebastian Mika et al. "Fisher discriminant analysis with kernels". In: *Neural networks for signal processing IX: Proceedings of the 1999 IEEE signal processing society workshop (cat. no. 98th8468)*. Ieee. 1999, pp. 41–48.

[28] Wolfgang HR Miltner, Christoph H Braun, and Michael GH Coles. "Event-related brain potentials following incorrect feedback in a time-estimation task: evidence for a "generic" neural system for error detection". In: *Journal of cognitive neuroscience* 9.6 (1997), pp. 788–798.

[29] Melody M Moore. "Real-world applications for brain-computer interface technology". In: *IEEE Transactions on Neural Systems and Rehabilitation Engineering* 11.2 (2003), pp. 162–165.

[30] Robert Oostenveld et al. "FieldTrip: open source software for advanced analysis of MEG, EEG, and invasive electrophysiological data". In: *Computational intelligence and neuroscience* 2011 (2011), p. 1.

[31] Adam Paszke et al. "Pytorch: Tensors and dynamic neural networks in python with strong gpu acceleration". In: *PyTorch: Tensors and dynamic neural networks in Python with strong GPU acceleration* 6 (2017).

[32] Gert Pfurtscheller and FH Lopes Da Silva. "Event-related EEG/MEG synchronization and desynchronization: basic principles". In: *Clinical neurophysiology* 110.11 (1999), pp. 1842–1857.

[33] John Polich. "Updating P300: an integrative theory of P3a and P3b". In: *Clinical neurophysiology* 118.10 (2007), pp. 2128–2148.

[34] Herbert Ramoser, Johannes Muller-Gerking, and Gert Pfurtscheller. "Optimal spatial filtering of single trial EEG during imagined hand movement". In: *IEEE transactions on rehabilitation engineering* 8.4 (2000), pp. 441–446.

[35] Brice Rebsamen et al. "A brain controlled wheelchair to navigate in familiar environments". In: *IEEE Transactions on Neural Systems and Rehabilitation Engineering* 18.6 (2010), pp. 590–598.

[36] Audrey S Royer et al. "EEG control of a virtual helicopter in 3-dimensional space using intelligent control strategies". In: *IEEE Transactions on neural systems and rehabilitation engineering* 18.6 (2010), pp. 581–589.

[37] Gerwin Schalk and Eric C Leuthardt. "Brain-computer interfaces using electrocorticographic signals". In: *IEEE reviews in biomedical engineering* 4 (2011), pp. 140–154.

[38] Gerwin Schalk et al. "Two-dimensional movement control using electrocorticographic signals in humans". In: *Journal of neural engineering* 5.1 (2008), p. 75.

[39] RT Schirrmeister et al. "Deep learning with convolutional neural networks for brain mapping and decoding of movement-related information from the human EEG. arXiv, 2017". In: *arXiv preprint arXiv:1703.05051* ().

[40] Bernhard Scholkopf and Alexander J Smola. *Learning with kernels: support vector machines, regularization, optimization, and beyond*. MIT press, 2001.

[41] Nitish Srivastava et al. "Dropout: a simple way to prevent neural networks from overfitting". In: *The Journal of Machine Learning Research* 15.1 (2014), pp. 1929–1958.

[42] Kazuo Tanaka, Kazuyuki Matsunaga, and Hua O Wang. "Electroencephalogram-based control of an electric wheelchair". In: *IEEE transactions on robotics* 21.4 (2005), pp. 762–766.

[43] Michael Tangermann et al. “Review of the BCI competition IV”. In: *Frontiers in neuroscience* 6 (2012), p. 55.

[44] Yogatheesan Varatharajah et al. “Integrating artificial intelligence with real-time intracranial EEG monitoring to automate interictal identification of seizure onset zones in focal epilepsy”. In: *Journal of neural engineering* 15.4 (2018), p. 046035.

[45] Meel Velliste et al. “Cortical control of a prosthetic arm for self-feeding”. In: *Nature* 453.7198 (2008), p. 1098.

[46] Yijun Wang, Shangkai Gao, and Xiaornog Gao. “Common spatial pattern method for channel selection in motor imagery based brain-computer interface”. In: *2005 IEEE Engineering in Medicine and Biology 27th Annual Conference*. IEEE. 2006, pp. 5392–5395.

Appendix A

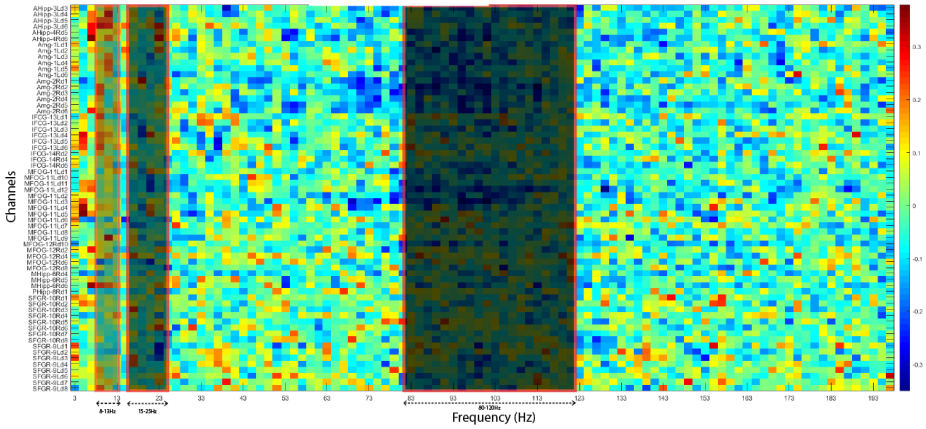

(a) Hilbert Power difference between left and right-hand movement as a function of frequency at all channels in subject CAR 10. The figure also shows the three selected frequency ranges of interest

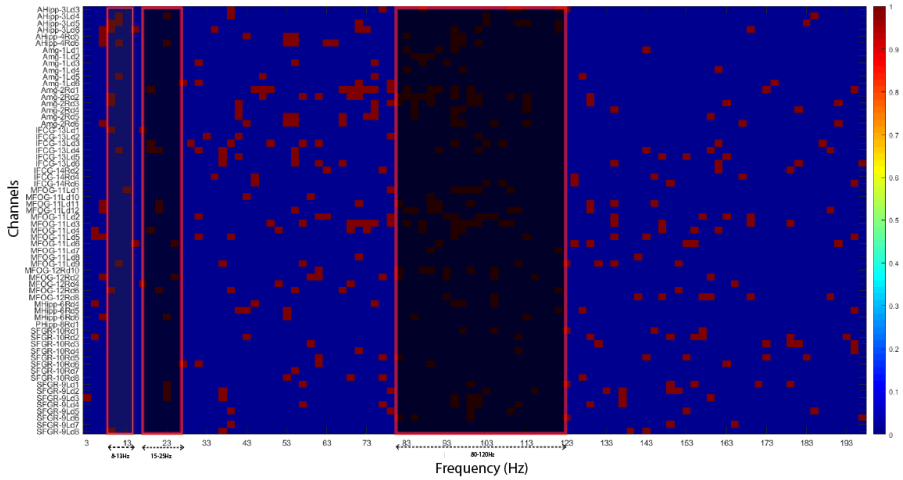

(b) Significant Hilbert Power difference between left and right-hand movements as a function of frequency at all channels in subject CAR 10. The red values indicate significant differences.

Figure A.1: CAR 10 Hilbert power and Hilbert Power Significance plots

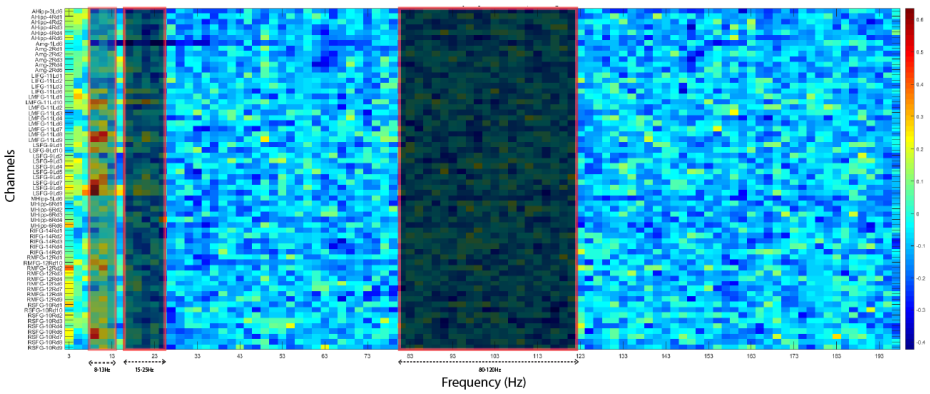

(a) Hilbert Power difference between left and right-hand movement as a function of frequency at all channels in subject CAR 08. The figure also shows the three selected frequency ranges of interest

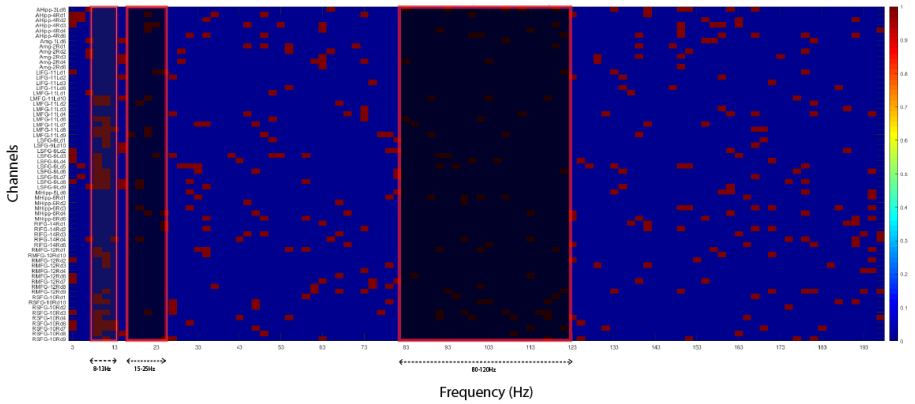

(b) Significant Hilbert Power difference between left and right-hand movements as a function of frequency at all channels in subject CAR 08. The red values indicate significant differences.

Figure A.2: CAR 08 Hilbert power and Hilbert Power Significance plots